Structural basis of diverse membrane target recognitions by ankyrins

Chao Wang, Zhiyi Wei, Keyu Chen, Fei Ye, Cong Yu, Vann Bennett, Mingjie Zhang

DOI: http://dx.doi.org/10.7554/eLife.04353

Cite as: eLife 2014;10.7554/eLife.04353

Received: 13 August 2014
Accepted: 7 November 2014
Published: 10 November 2014

Structural Basis of Diverse Membrane Target Recognitions by Ankyrins

Chao Wang[1,6], Zhiyi Wei[1,2,3,6], Keyu Chen[1], Fei Ye[1], Cong Yu[1,3], Vann Bennett[4,5], and Mingjie Zhang[1,2,*]

[1]Division of Life Science, State Key Laboratory of Molecular Neuroscience,

[2]Center of Systems Biology and Human Health, School of Science and Institute for Advanced Study,

Hong Kong University of Science and Technology, Clear Water Bay, Kowloon,

Hong Kong, China.

[3]Department of Biology, South University of Science and Technology of China, Shenzhen, China.

[4]Howard Hughes Medical Institute,

[5]Departments of Biochemistry, Cell Biology, and Neurobiology,

Duke University Medical Center, Durham, North Carolina 27710, USA.

Running title: Ankyrin repeats/target complex structures

[6]These authors contributed equally to this work.

*Correspondence to: mzhang@ust.hk

Abstract

Ankyrin adaptors together with their spectrin partners coordinate diverse ion channels and cell adhesion molecules within plasma membrane domains and thereby promote physiological activities including fast signaling in the heart and nervous system. Ankyrins specifically bind to numerous membrane targets through their 24 ankyrin repeats (ANK repeats), although the mechanism for the facile and independent evolution of these interactions has not been resolved. Here we report the structures of ANK repeats in complex with an inhibitory segment from the C-terminal regulatory domain and with a sodium channel Nav1.2 peptide, respectively, showing that the extended, extremely conserved inner groove spanning the entire ANK repeat solenoid contains multiple target binding sites capable of accommodating target proteins with very diverse sequences via combinatorial usage of these sites. These structures establish a framework for understanding the evolution of ankyrins' membrane targets, with implications for other proteins containing extended ANK repeat domains.

Introduction

Ankyrins are a family of scaffold proteins playing essential roles in connecting numerous ion channels, cell adhesion molecules and receptors to the spectrin-based cytoskeleton beneath membranes and thereby provide mechanical support of plasma membranes and control activities of excitable tissues including neurons and muscles (Bennett and Chen, 2001; Bennett and Healy, 2009). Human ankyrins contain three members, ankyrin-R/B/G (AnkR/B/G), encoded by *ANK1/2/3*, respectively. They all consist of a highly similar N-terminal membrane binding domain composed of 24 ANK repeats, a spectrin binding domain comprised of two ZU5 domains and a UPA domain followed by a death domain (DD), and a variable C-terminal regulatory domain (Bennett and Lorenzo, 2013) (Figure 1A). Although sharing similar domain organizations, the three ankyrins have distinct and non-overlapping functions in specific membrane domains coordinated by ankyrin-spectrin networks (Abdi et al., 2005; He et al., 2013; Mohler et al., 2002). As an adaptor protein linking membrane proteins to the underlying cytoskeleton, dysfunction of ankyrins are closely related to serious human diseases. For example, loss-of-function mutations of ankyrins can cause hemolytic anemia (Gallagher, 2005), various cardiac diseases including several cardiac arrhythmia syndromes and sinus node dysfunctions (Hashemi et al., 2009; Le Scouarnec et al., 2008; Mohler et al., 2007; Mohler et al., 2003), bipolar disorder (Dedman et al., 2012; Ferreira et al., 2008; Rueckert et al., 2013) and autism spectrum disorders (Iqbal et al., 2013; Shi et al., 2013).

The wide-ranging physiological functions of ankyrins are manifested by ankyrin's remarkable capacity in binding to and anchoring numerous membrane targets, via their N-terminal 24 ankyrin repeats, to specific membrane micro-domains in coordination with spectrin-based cytoskeletal structures (Bennett and Chen, 2001). One good example is the formation and maintenance of axon initial segments (AIS) in neurons. Interaction between AnkG and L1 cell adhesion molecules (e.g. the 186-kDa

neurofascin, referred to as Nfasc in this study) is required for formation and stability of the AIS (Hedstrom et al., 2007; Zonta et al., 2011). AnkG is in turn responsible for clustering voltage-gated sodium channels at the AIS, which underlies the mechanistic basis of action potential generation and propagation (Garrido et al., 2003; Kole et al., 2008)(see review (Rasband, 2010)). Anchoring of L1 cell adhesion molecules also directs inhibitory GABAergic synapse innervation at the AIS of excitatory Purkinje neurons (Ango et al., 2004), a critical step for balanced neuronal circuit formation. Depletion of AnkG both in cultured hippocampal neurons and in mice causes axons to lose axonal properties and acquire the molecular characteristics of dendrites, showing that AnkG is required for maintenance of axonal polarity (Hedstrom et al., 2008; Sobotzik et al., 2009).

Other examples of ankyrins function in organizing membrane signaling network include, but not limit to, AnkB/G-mediated coordination of voltage-gated sodium channels, Na/K ATPase, Na/Ca exchanger, and inositol 1,4,5-triphosphate receptors in cardiomyocytes (Hund et al., 2008; Lowe et al., 2008; Mohler et al., 2005; Mohler et al., 2004) and the dystrophin/dystroglycan complex in skeletal muscles (Ayalon et al., 2008; Ayalon et al., 2011). Finally, as it was originally discovered (Bennett and Stenbuck, 1979a, b), AnkR is well-known to be essential for preserving erythrocyte membrane integrity. Although the critical functions of ankyrins in the specialized membrane domains have been recognized for decades, the underlying mechanistic basis governing ankyrin's coordination with such broad spectrum of membrane targets remains essentially unknown, largely due to challenges in characterizing biochemical and structural properties of the elongated ankyrin repeats. Additionally, it is noted that the ankyrin repeats of ankyrins have been extremely conserved, whereas the membrane targets continue to expand throughout the evolution, presumably due to functional requirements for membrane microdomain-mediated fast signaling events in higher eukaryotes including mammals.

In this study, we performed detailed biochemical characterizations of ANK repeats of ankyrins and their interactions with various binding partners. We solved the

crystal structures of ANK repeats in complex with an auto-inhibitory segment from AnkR C-terminal domain and with a peptide from Nav1.2, respectively. The 24 ANK repeats of ankyrins form a superhelical solenoid with an extremely conserved elongated inner groove, which contains multiple quasi-independent target binding sites. We further show that ankyrins can accommodate different membrane targets with diverse sequences by combinatorial usages of these binding sites. The ankyrin-Nav1.2 complex structure also provides a mechanistic explanation of the mutation found in Nav channels that cause cardiac diseases in humans. Collectively, our findings provide the first glimpse into the mechanistic basis governing membrane target recognition by the highly conserved ANK repeats in ankyrins and set up a structural framework for future investigation of ankyrin's involvement in physiological functions and pathological conditions in diverse tissues. Our results also provide a molecular mechanism for the rapid expansion of ankyrin partners in vertebrate evolution. These insights also will be valuable for understanding recognition mechanisms of other long ANK repeats proteins as well as many other long repeat-containing proteins in living kingdoms in general.

Results

An auto-inhibitory segment from the C-terminal domain of AnkR specifically binds to ANK repeats of ankyrins

To elucidate the mechanisms governing ANK repeat-mediated binding of ankyrins to diverse membrane targets, we attempted to determine the atomic structures of ANK repeats alone or in complex with their targets. However, extensive trials of crystallizing ANK repeat domains of AnkR/B/G were not successful, presumably due to the highly dynamic nature of the extended ANK repeat solenoid (Howard and Bechstedt, 2004; Lee et al., 2006). Anticipating that ANK repeats binders may rigidify the conformation of ANK repeats, we turned our attention to the ANK repeat/target complexes. The C-terminal regulatory domains have been reported

to bind to ANK repeats intra-molecularly and modulate the target binding properties of ankyrins (Abdi et al., 2005; Davis et al., 1992). We measured the interaction of AnkR_repeats with its entire C-terminal regulatory domain (residues 1529-1907) using highly purified recombinant proteins, and found that they interact with each other with K_d around 1 μM (Figure 1B). It is expected that the intra-molecular association between ANK repeats and its C-terminal tail of AnkR is very stable, and thus the full-length AnkR likely adopts an auto-inhibited conformation and ANK repeats-mediated binding to membrane targets requires release of the auto-inhibited conformation of AnkR.

Via isothermal titration calorimetry (ITC)-based quantitative binding assays, we identified a 48-residue auto-inhibitory segment (residues 1577-1624, referred to as "AS") as the complete ANK repeat-binding region (Figure 1B, C). Further truncation at the either end of this 48-residue AS fragment significantly decreased its binding to AnkR_repeats (Figure 1B). The corresponding sequence does not exist in AnkB or AnkG, indicating the AS is specific to AnkR (Figure 1A). AnkR_AS was found to bind to AnkR/B/G ANK repeats with comparable affinities (Figure 1D), as expected since AnkR/B/G share extremely conserved ANK repeats sequences (Figure 2B and see below). Thus, we tried the complexes of AnkR_AS with ANK repeats of all three isoforms to increase chances of obtaining suitable crystals. Although crystals of various complexes were obtained, they all diffracted very poorly. After extensive trails of screening and optimization, we succeeded in obtaining good-diffraction crystals of AnkR_AS fused at its C-terminus with the AnkB_repeats and solved the structure of the fusion protein at 3.5-Å resolution (Figure 2C and Table 1). NMR spectra of the $^{13}CH_3$-Met selectively labeled fusion protein and the ANK repeats/AS complex produced by cleavage of the fusion protein at the fusion site are essentially identical (Figure 2-figure supplement 1), indicating that the fusion strategy used here facilitates crystallization but does not alter the structure of the ANK repeats/AS complex. There are three Met residues in AS (Met1601, Met1604 and Met1607) and all three Met residues are in the binding interface between ANK repeats and AS (Figure 2-figure supplement 2A).

Overall structure of the AnkB_repeats/AnkR_AS complex

Except for a few connecting loops and termini of the chains, the rest of the ANK repeats and AS are properly defined (Figure 2C and Figure 2-figure supplement 2). The 24 ANK repeats form a left-handed helical solenoid with each repeat rotating anti-clockwise by ~16˚ (Figure 2C). Except for the capping helices in the first and last repeats (i.e. αA of R1 and αB of R24), each repeat has the typical ANK repeat sequence pattern and forms a helix-turn-helix conformation (Figure 2A, C). A well-defined finger-like hairpin loop (finger loop) connects two consecutive repeats. The inner αA helices and the finger loops of the 24 repeats line together to form an elongated concave inner groove, and the αB helices of the repeats form the solvent exposed convex outer surface. The ANK repeats superhelix has the outer and inner diameters of approximate 60 Å and 45 Å, respectively, and the total height of ~150 Å (Figure 2C). The size of the ANK repeats revealed here is consistent with the previous measurement by atomic force microscopy (Lee et al., 2006). The C-terminal half of the ANK repeats structure aligns well with the apo-form structure of the last 12 ANK repeats of AnkR with overall RMSD of 1.6 Å (Michaely et al., 2002).

We analyzed the amino acid residues at each position of vertebrate AnkR/B/G ANK repeats and found that at most of positions the conservation is higher than 80% (Figure 2B and Figure 2-figure supplement 3). Further analysis reveals that residues forming the target binding concave inner groove (i.e. residues of the finger loops and αA helices of the 24 repeats) are essentially identical among vertebrate AnkR/B/G (Figure 2B and Figure 2-figure supplement 3), indicating that both the structure and the target binding properties of their ANK repeats are likely to be the same (also see Figure 1D). Additionally, the residues in the entire inner groove of ANK repeats superhelix are highly conserved for all ankyrins throughout the evolution (from worm to human) (Figure 2D and Video 1), suggesting that the functions of ANK repeats in different species of ankyrins are highly conserved during the evolution and that the inner groove of ANK repeats is the general binding site for membrane-associated targets of ankyrins. Consistent with this prediction, binding of AS to AnkG_repeats

prevents voltage-gated sodium channel Nav1.2 and Nfasc from binding to AnkG (Figure 3-figure supplement 1). Therefore, we hypothesized that the ANK repeats/AS structure presented here serves as a general framework for understanding how ankyrins engage their membrane targets, and tested this hypothesis using mutations designed and tested as described below.

Before binding to ANK repeats, AS adopts a random coil structure as indicated by its NMR spectrum (data not shown). In the complex, AS adopts a highly extended structure binding to part of the inner groove formed by the N-terminal 14 ANK repeats (R1-14) with its chain orientation antiparallel to that of ANK repeats (Figure 2A, C). A 10-residue segment of AS (residues 1592-1601) forms an α-helix when bound to ANK repeats (Figure 2C). The residues connecting AS and ANK repeats (10 residues in total, "GSLVPRGSGS") are flexible, indicating that the fusion of the two chains together does not introduce obvious conformational restrains to the complex.

The binding of AS to ANK repeats can be divided somewhat arbitrarily into three sites (site-1, 2, and 3) formed by the repeats 2-6, 7-10, and 11-14, respectively (Figure 2C and Figure 3A-C). Nonetheless, this division is supported by several lines of evidences. Structurally, there is a fairly clear boundary between each of the two binding sites in the ANK repeats/AS complex structure; whereas the interactions within each sites are rather concentrated (Figure 3). The most direct evidence is from the interaction between ANK repeats and Nav1.2 (see below). In the case of Nav1.2 binding, R1-6 of ANK repeats binds to the C-terminal half of the Nav1.2_ABD (ankyrin binding domain) and R11-14 binds to N-terminal half of Nav1.2_ABD. R7-10 is not involved in the Nav1.2 binding. Thus, one can naturally divide ANK repeats R1-14 into three parts. Such division is further supported by the well accepted concept that 4-5 ankyrin repeats can form a folded structural unit. In our case, the sites-2&3 contain 4 repeats each, and the site-1 contains 5 repeats if we do not count the capping repeat 1.

The interactions in the site-1 are primarily charge-charge and hydrogen bonding in nature, although hydrophobic contacts also contribute to the binding (Figure

3A). The interactions in the site-2 are mediated both by hydrophobic and hydrogen bonding interactions, and interactions in site-3 are mainly hydrophobic (Figure 3B, C). The structure of the ANK repeats/AS complex is consistent with the idea that ANK repeats bind to relatively short and unstructured peptide segments in ankyrins' membrane targets (Bennett and Healy, 2009; Bennett and Lorenzo, 2013).

Ankyrins bind to Nav1.2 and Nfasc through combinatorial usage of multiple binding sites

We next dissected the interactions of AnkG_repeats with Nav1.2 and Nfasc using the structure of the ANK repeats/AS complex to design mutations specifically affecting each predicted site. The K_d of the binding of AnkG_repeats to the Nav1.2 ankyrin-binding domain (ABD) (residues 1035-1129, comprising the majority of the cytoplasmic loop connecting transmembrane helices II&III, see below for details) and to the Nfasc ABD (a 28-residue fragment in the cytoplasmic tail, Figure 3-figure supplement 2 and see (Garver et al., 1997)) is 0.17 and 0.21 μM, respectively (Figure 3E upper panels). To probe the binding sites of Nav1.2 and Nfasc on AnkG, we constructed AnkG_repeat mutants with the corresponding hydrophobic residues in the binding site-1 (Phe131 and Phe164 in R4 and R5; termed as "FF"), site-2 (Ile267 and Leu300 in R8 and R9; "IL"), and site-3 (Leu366, Phe399, and Leu432 in R11, R12, and R13; "LFL") substituted with Gln (Figure 3D), and assayed their binding to the two targets. The mutations in the site-1 significantly decreased ANK repeat binding to Nav1.2, but had no impact on the Nfasc binding. Conversely, the mutations in the site-2 had minimal impact on Nav1.2 binding, but significantly weakened Nfasc binding. The mutations in the site-3 weakened ANK repeat binding to both targets (Figure 3F, Figure 3-figure supplement 3 and Figure 3-figure supplement 4). The above results indicate that the two targets bind to ANK repeats with distinct modes with Nav1.2 binding to the sites-1&3 and Nfasc binding to the sites-2&3. This conclusion is further supported by the binding of the two targets to various AnkG_repeat truncation mutants (Figure 3F, Figure 3-figure supplement 3 and Figure 3-figure supplement 4).

We have also assayed the impact of the mutations of the three sites on the binding of AnkR_AS to ANK repeats. The mutations in site-1 and -2 led to ~20-fold decrease of AnkR_AS binding, and the site-3 mutation only caused ~3-fold decrease of AnkR_AS binding (Figure 4A). Finally, we tested the bindings of another two reported ankyrin targets, the KCNQ2 potassium channel (Pan et al., 2006) and the voltage-gated calcium channel Cav1.3 (Cunha et al., 2011), to the ANK repeats and its mutants, and found that KCNQ2 mainly binds to the sites-1&2, and Cav1.3 primarily relies on site-2 of ANK repeats (Figure 4B, C). Taken together, the above biochemical analysis together with the structure of the ANK repeats/AS complex reveals that through combinations of multiple binding sites on the extremely conserved and elongated inner groove formed by the 24 ANK repeats, ankyrins can bind to numerous targets with diverse amino acid sequences. It is likely that some ankyrin targets may bind to the groove formed by the rest of the repeats in addition to R1-14.

An elongated fragment of Nav1.2 binds to ANK repeats

To further delineate the target binding mechanisms of ankyrins, we characterized the interaction between AnkG_repeats and Nav1.2 in detail. Previous studies have reported that the intracellular loop connecting the transmembrane helices II&III (loop 2) is responsible for targeting Nav1.2 to axon initial segment via directly binding to AnkG, and identified a 27-residue motif within the loop 2 ("ABD-C" indicated in Figure 5A, D) as the AnkG binding domain (Garrido et al., 2003; Lemaillet et al., 2003). First, we confirmed that a 95-residue fragment (ABD, residues 1035-1129; Figure 5D) is sufficient for binding to AnkG (Figure 3E upper left panel). Surprisingly, we found that the C-terminal part of the ABD (ABD-C, the 27-residue motif identified previously for ANK repeats binding) binds to ANK repeats with an affinity ~15-fold weaker than the entire ABD, indicating that the ABD-C is not sufficient for binding to ANK repeats (Figure 5B, C). Consistent with this observation, the N-terminal 68-residue fragment of the loop 2 (ABD-N, residues 1035-1102) also binds to ANK repeats, albeit with a relatively weak affinity (K_d of ~8 μM; Figure 5B, C). We further showed that the ABD-C fragment binds to the repeats 1-6 (R1-6) of

ANK repeats, as ABD-C binds to R1-6 and the entire 24 ANK repeats with essentially same affinities (Figure 5B, C). These results also reveal that, like the AnkR_AS, the Nav1.2 peptide segment binds to ANK repeats in an anti-parallel manner. Taken together, the biochemical data shown in Figure 3E and Figure 5 indicate that two distinct fragments of Nav1.2 loop 2, ABD-N and ABD-C, are responsible for binding to ANK repeats. The previously identified ABD-C binds to the site-1 and ABD-N binds to the site-3 of ANK repeats, and the interaction between the two sites are largely independent from each other energetically.

We noted from the amino acid sequence alignment of the Nav1 members that the sequences of ABD-C (the first half in particular) are much more conserved than those of ABD-N (Figure 5D). Further mapping experiments showed that the C-terminal less-conserved 10 residues of ABD-C are dispensable for Nav1.2 to bind to ANK repeats (Figure 5B, top two rows). Truncations at the either end of Nav1.2 ABD-N weakened its binding to ANK repeats (data not shown), indicating that the entire ABD-N is required for the channel to bind to the site-3 of ANK repeats. The diverse ABD-N sequences of Nav1 channels fit with the relatively non-specific hydrophobic-based interactions in the site-3 observed in the structure of ANK repeats/AS structure (Figure 3C).

Structure of Nav1.2_ABD-C/AnkB_repeats_R1-9 reveals binding mechanisms

Although with very low amino acid sequence similarity, the Nav1.2_ABD-C (as well as the corresponding sequences from Nav1.5, KCNQ2/3 potassium channels, and β-dystroglycan (Ayalon et al., 2008; Mohler et al., 2004; Pan et al., 2006)) and the site-1 binding region of AnkR_AS share a common pattern with a stretch of hydrophobic residues in the first half followed by a number of negatively charged residues in the second half (Figure 6C). Based on the structure of the ANK repeats/AS complex, we predicted that the Nav1.2_ABD-C may also bind to the site-1 of AnkG_repeats with a pattern similar to the AS peptide. We verified this prediction by determining the structure of a fusion protein with the first 9 ANK repeats of AnkB

fused at the C-terminus of Nav1.2_ABD-C at 2.5-Å resolution (Figure 6A, Figure 6-figure supplement 1 and Table 1; the ANK repeats/the entire ABD complex crystals diffracted very poorly presumably due to the flexible nature of the interaction between Nav1.2_ABD-N and the site-3 of ANK repeats).

In the complex structure, the extended Nav1.2_ABD-C peptide interacts with the surface of the inner groove formed by the first five ANK repeats (Figure 6A). In particular, the hydrophobic residues of Nav1.2_ABD-C and AS occupy very similar positions on the hydrophobic groove formed by residues from ANK repeats R4&5, and subtle conformational differences in the finger loops of R4 and R5 can accommodate amino acid sequence differences between the two targets (Figure 6E). This similar pattern and subtle accommodation illustrate that ANK repeats in general are incredibly adaptable and versatile as protein binding modules. Unique to Nav1.2, the binding of ABD-C extends all the way to R1 via charge-charge and hydrogen-bond interactions (Figure 6A, E). We also compared our ANK repeats complex structure with two recently determined peptide-bound ANK repeats structures, ANKRA2 and RFXANK in complex with HDAC4 and RFX5 peptides, respectively (Xu et al., 2012). Although the HDAC4 and RFX5 peptides also bind to ANKRA2 and RFXANK ankyrin repeats in extended conformations, the key target binding residues are restricted to a small set of hydrophobic residues in the A-helices of the 5 ankyrin repeats. Accordingly, a consensus sequence motif can be recognized to bind to the ANKRA2 and RFXANK ankyrin repeats.

A completely conserved Glu in ABD-C anchors Nav1 to ankyrins

We noted that Glu1112, which is completely conserved in both Na+- and K+-channels and mutation of which in Nav1.5 to Lys is known to cause Brugada syndrome in humans (Mohler et al., 2004), occupies the identical position as Glu1622 of AS does in the ANK repeats/AS complex (Figure 3A and Figure 6A, E). In contrast to the common expectation of directly interacting with positively charged residue(s), Glu1112 of Nav1.2 buries deeply into the groove and forms hydrogen bonds with the

sidechains of Thr94 and Asn98 in the R2&3 finger loop (Figure 6A). Charge potential calculation shows that the Glu1112 binding pocket formed by R2&3 is highly positive, and thus nicely accommodate the negatively charged carboxyl group of Glu1112 (Figure 6B). As expected, the charge reversal mutation of Nav1.2 (E1112K) abolished the channel's binding to ANK repeats. Even mild substitutions (E1112Q- and E1112A-Nav1.2) weakened the binding of Nav1.2 to ANK repeats by ~30 fold (Figure 6D). Fitting with our findings, E1112Q- and E1112A-Nav1.2 (or E1100 in Nav1.6) failed to cluster at AIS of hippocampal neurons (Fache et al., 2004; Gasser et al., 2012). Conversely, substitutions of Thr94 and Asn98 of ANK repeats with Ala and Glu, respectively, also weakened the ANK repeats/Nav1.2_ABD interaction (Figure 6D). The above biochemical and structural data illustrate the importance of the absolutely conserved Glu in various ankyrin binding targets shown in Figure 5D and Figure 6C in anchoring these binding domains to the site-1 of ANK repeats. The structures of ANK repeats in complex with the two different targets shown here also provide a framework for understanding the binding of KCNQ2/3, β-dystroglycan, and potentially other ankyrin partners.

AnkG-mediated clustering of Nfasc and Nav channels at AIS

We next evaluated consequences of mutations of AnkG characterized in Figure 3 on its function in clustering Nav channels and Nfasc at the axon initial segment in cultured hippocampal neurons. It is predicted that the "FF" mutant in the site-1 of AnkG repeats should disrupt its Nav1.2 binding but retain the Nfasc binding (Figure 3F). As shown previously (He et al., 2012), the defect of both AIS formation and Nav channels/Nfasc clustering at AIS caused by knockdown of endogenous AnkG could be rescued by co-transfection of the shRNA-resistant, WT 270-kDa AnkG-GFP (Figure 7). The "FF" mutant of 270-kDa AnkG-GFP was concentrated normally at AIS, but failed to rescue clustering of endogenous Nav at the AIS (Figure 7A, C, D), consistent with the significantly weakened binding of the mutant AnkG to Nav1.2 (Figure 3E, F). This result confirms that the proper clustering of Nav at the AIS depends on AnkG

(Garrido et al., 2003; Zhou et al., 1998). In contrast, Nfasc clustered properly at AIS in neurons co-transfected with "FF"-AnkG (Figure 7B, E), which was predicted since the "FF" mutant had no impact on AnkG's binding to Nfasc. Interestingly, both the "IL"- (site-2) and "LF"- (part of site-3) mutants of AnkG-GFP failed to cluster at AIS of hippocampal neurons (Figure 7C and Figure 7-figure supplement 1), suggesting that the L1-family members (Nfasc and/or Nr-CAM) or other potential ANK repeats site-2/3 binding targets may play a role in anchoring AnkG at the AIS. Not surprisingly, neither of these mutants can rescue the clustering defects of Nav or Nfasc caused by the knockdown of endogenous AnkG (Figure 7D, E and Figure 7-figure supplement 1).

Discussion

Ankyrins are very ancient scaffold proteins present in their modern form in bilaterian animals with their functions greatly expanded in vertebrate evolution (Bennett and Lorenzo, 2013; Cai and Zhang, 2006; Hill et al., 2008). Gene duplications as well as alternative splicing have generated much functional diversity of ankyrins in various tissues in vertebrates. However, the N-terminal 24 ANK repeats of ankyrins have remained essentially the same for at least 500 million years (Figure 2B and Figure 2-figure supplement 3). In contrast, the membrane targets for ankyrins have expanded greatly in respond to physiological needs (e.g. fast signaling in neurons and heart muscles in mammals) throughout the evolution, and these membrane targets almost invariably bind to the 24 ANK repeats of ankyrins. Intriguingly, among about a dozen of ankyrin-binding membrane targets identified to date (see review (Bennett and Healy, 2009)) and the ones that characterized in this study, the ankyrin-binding sequences of these targets are highly diverse. It has been unclear how the extremely conserved ANK repeats can specifically bind to such diverse set of target sequences. Additionally, it is mechanistically unclear why the membrane targets instead of ANK repeats have undergone amino acid sequence changes in respond to functional diversification in high vertebrates during the evolution. The structure of the entire 24 ANK repeats in complex with an

auto-inhibitory domain, together with the structure of part of ANK repeats in complex with its binding domain of Nav1.2, begin to offer insights into above questions.

Ankyrin's diverse membrane targets

The 24 ANK repeats form an elongated, continuous solenoid structure with its extremely conserved target binding inner groove spanning a total length of ~210 Å (Figure 2C). We identified three distinct target binding sites in the first 14 repeats (Figure 2 and Figure 3). This is in agreement with earlier studies showing that 3-5 ankyrin repeats can form a stable structural unit capable of recognizing certain target sequences (Li et al., 2006; Tamaskovic et al., 2012; Xu et al., 2012). Therefore, we predict that the last 10 ANK repeats of ankyrins can contain additional 2-3 target binding sites. Importantly, the target binding sites on ANK repeats behaves rather independently, as mutations/disruptions of interactions in each site do not lead to large perturbations on the interactions in the neighboring sites (Figure 3). Equal importantly, the ANK repeats targets bind to the inner groove with extended conformations, and the segments responsible for binding to each site do not seem to cooperate with each other (i.e. alteration in one segment does not have large impact on the neighboring segments) (Figure 3 and Figure 5). Therefore, the multiple target binding sites on ANK repeats are quasi-independent.

We further show that the AnkR_AS, the Nfasc, the Nav1.2, the KCNQ2, and the CaV1.3 peptides use different combinations of these sites that spread along the elongated and near completely conserved inner ANK repeat groove to form specific ankyrin/target complexes. One can envision that such combinatorial usage of multiple quasi-independent sites can in principle generate a large repertoire of binding targets with different sequences for ANK repeats. Although a number of ion-channels use the site-1 as the common binding site, the amino acid sequences of the corresponding site-1-binding peptide segments are rather diverse (Figure 6C). One can expect that the sequences of target peptide segments responsible for binding to the sites-2&3 will be even more diverse (e.g. the corresponding site-3 binding sequence of AnkR_AS

and Nav1.2 ABD_N have no detectable sequence similarity), as the interactions in these two sites are more hydrophobic in nature (Figure 3A-C). The combinatorial usage of the quasi-independent sites, together with the low sequence specificity of each binding site as well as the structural plasticity of the ANK repeat solenoid (Lee et al., 2006), indicate that ANK repeats can have large capacities in binding to numerous membrane targets with diverse sequences. With all above points in mind, unidentified ANK repeat binding proteins will likely be difficult to predict simply based on amino acid sequences, though a firm conclusion awaits detailed characterizations of more ankyrin binding targets.

The combinatorial usage of multiple binding sites have also been observed in other long repeat-containing proteins including the Karyopherin family nuclear import/export scaffold proteins (Chook and Blobel, 2001; Conti et al., 1998; Kobe, 1999; Xu et al., 2010), the Wnt signaling regulatory scaffold β-catenin (Graham et al., 2000; Huber and Weis, 2001), and tetratricopeptide repeats protein LGN/Pins (Zhu et al., 2011). It is possible such combinatorial target binding strategy may be a common feature for many other elongated repeat-containing proteins in diverse living organisms. The combinatorial multi-site interaction mode may also be advantageous for efficient regulation of ANK repeats/target interactions. By spreading a target binding to multiple sites along the ANK repeats inner groove that are not directly coupled, each binding site can be regulated independently and in a graded fashion. This might allow multiple regulatory signals to be integrated in a combinatorial manner to regulate ankyrin/membrane target interactions. Such graded regulatory mechanism can be important for ankyrins to respond to various signal inputs when multiple membrane targets co-exist. For example, AnkG co-exists with Nfasc and sodium and potassium channels at AIS (Jenkins and Bennett, 2001; Le Bras et al., 2013; Pan et al., 2006), and the components of the AnkG-mediated complex at AIS can undergo distinct activity-dependent changes (Grubb and Burrone, 2010; Hu et al., 2009; Kuba et al., 2010), reviewed in (Kole and Stuart, 2012)) and exhibit the AIS plasticity during development (Galiano et al., 2012; Gutzmann et al., 2014). It has been reported that Nfasc and sodium channels can undergo activity-dependent

phosphorylation in their ANK repeat binding domains (Brechet et al., 2008; Garver et al., 1997; Whittard et al., 2006), which may underlie the distinct patterns of concentration gradients and their activity-dependent changes along AIS.

Evolution implications of multiple membrane targets of ankyrins

The target binding inner groove of ANK repeats of ankyrins essentially has not changed ever since the protein was born over 500 million years ago. In contrast, most, if not all, currently identified ANK repeat-binding segments of ankyrin's membrane targets are either shown or predicted to be unstructured before binding to ankyrins (Bennett and Lorenzo, 2013). Such unstructured sequences are more tolerant to mutations as alterations are likely to have minimal impact on the overall folding of proteins harboring them. Additionally, the conformational malleability is also advantageous for these unstructured peptide sequences to bind to ANK repeats with a molded groove. Since ANK repeats of ankyrins are responsible for binding to numerous targets with diverse sequences, it is likely that there exists an evolution pressure against random mutations in the ANK repeat sequences (the residues in the inner groove in particular). The core function of the ankyrin/spectrin duo in patterning membrane micro-domains remains unchanged throughout the evolution, and thus the amino acid sequences of ANK repeats and spectrin-binding domain of ankyrins are highly conserved (Wang et al., 2012). New ankyrin binders (e.g. sodium and potassium channels at AIS of neurons of higher mammals) can be evolved due to functional requirements.

In summary, the structure of the 24 ANK repeats of ankyrins not only offers an explanation to AnkR/B/G's remarkable capacity in binding to numerous membrane targets, but also provides a framework for guiding future studies of physiological functions and numerous pathological conditions directly associated with ankyrins. Since the three isoforms of ankyrins have distinct physiological functions, highly variable sequences outside the extremely conserved ANK repeats and spectrin binding domain likely play critical roles in determining the cellular functions of each ankyrin

isoform. Finally, proteins with extended ankyrin repeat domains (e.g., TRP channels, elongation factors, protein kinases and phosphatases, and various scaffold proteins) may also interact with diverse partners via combinatorial uses of multiple, quasi-independent binding sites and thus are particularly suited as adaptors for assembling macromolecular complexes with broad cellular functions.

Materials and methods

Constructs, protein expression and purification

The coding sequences of AnkB_repeats (residues 28-873) were PCR amplified using the full-length human 220-kDa AnkB as the template. The coding sequences of the AnkR constructs, including AnkR_repeats (residues 42-853), and the full length AnkR C-terminal domain (residues 1529-1907), were PCR amplified from a mouse muscle cDNA library. The coding sequence of AnkG_repeats (residues 38-855) were PCR amplified using the full-length rat 190-kDa AnkG as the template. The fusion construct of AnkR_AS and AnkB_repeats was made by standard two-step PCR with a coding sequence of thrombin recognition residues "GSLVPRGS" as the linker. This construct was used to crystallize and determine of the complex structure. The same strategy was used in making other fusion constructs, including the Nav1.2_ABD-C/AnkB_repeats_R1-9 fusion construct containing residues 1103-1129 from mouse Nav1.2 and human AnkB residues 28-318 followed by a capping sequence corresponding to the αB of R24 (residues 814-822) and the AnkR_AS/AnkG_repeats fusion construct. For truncation mutations of ANK repeats constructs, the same capping sequence was added to the appropriate region of the C-terminus of each construct for protein stabilization. Mouse Nav1.2 (NP_001092768.1) and mouse neurofascin (CAD65849.1) were used here for studying their interaction with ankyrins. Peptides for mouse KCNQ2 (NP_034741.2, residues 826-845) and mouse Cav1.3 (NP_083257.2, residues 2134-2166) were synthesized from company. For simplicity, we used human 220-kDa AnkB for the

amino acid numbering throughout the manuscript. If the corresponding point mutations were made on AnkG_repeats, each of the residue numbering should be shifted to a larger number by ten residues. All point mutations were created using the Quick Change site-directed mutagenesis kit and confirmed by DNA sequencing. All of these coding sequences are cloned into a home-modified pET32a vector for protein expression. The N-terminal thioredoxin-His_6-tagged proteins were expressed in *Escherichia coli* BL21 (DE3) and purified as previous described (Wang et al., 2012). The thioredoxin-His_6-tag was removed by incubating with HRV 3C protease and separated by size exclusion columns when needed.

Isothermal Titration Calorimetry assay

Isotermal titration calorimetry (ITC) measurements were carried out on a VP-ITC Microcal calorimeter (Microcal) at 25℃. All proteins were in 50 mM Tris buffer containing 100 mM NaCl, 1 mM EDTA and 1 mM DTT at pH 7.5. High concentration (200-300 μM) of each binding partners assayed in this study, including AS of AnkR, different Nav1.2 ABD proteins and mutants, and neurofascin ABD, were loaded into the syringe, with the corresponding ankyrin repeats proteins of ankyrin-R/B/G (20-30 μM) in the cell. Each titration point was performed by injecting a 10 μL aliquot of syringe protein into various ankyrin protein samples in the cell at a time interval of 120 seconds to ensure that the titration peak returned to the baseline. The titration data were analyzed using the program Origin7.0 and fitted by the one-site binding model.

Analytical gel filtration

Analytical gel filtration chromatography was carried out on an AKTA FPLC system (GE Healthcare). Proteins were loaded onto a Superose 12 10/300 GL column (GE Healthcare) equilibrated with a buffer containing 50 mM Tris, 100 mM NaCl, 1 mM EDTA and 1 mM DTT at pH 7.5.

Fluorescence assay

Fluorescence assays were performed on a PerkinElmer LS-55 fluorimeter equipped with an automated polarizer at 25 °C. In a typical assay, a FITC (Molecular Probes) -labeled peptide (~ 1 μM) was titrated with each binding partner in a 50 mM Tris pH 8.0 buffer containing 100 mM NaCl, 1 mM DTT, and 1 mM EDTA. The K_d values were obtained by fitting the titration curves with the classical one-site binding model.

NMR spectroscopy

For the purpose of NMR analysis, AnkB_repeats fused with AnkR_AS was prepared by growing bacterial in M9 minimal medium supplemented with $^{13}CH_3$-Met (CIL, Cambridge, MA). The protein was expressed and purified using the same method as for the native proteins. Two identical NMR samples containing 0.35 mM of the fusion protein in 50 mM Tris buffer (pH 7.0, with 100 mM NaCl, 1 mM DTT, 1mM EDTA) were prepared, except that one of the sample contained 50μg/mL of thrombin. The complete cleavage of the fusion protein was assessed by taking a small aliquot thrombin-added sample for SDS-PAGE analysis. NMR spectra were acquired at 35 °C on a Varian Inova 750 MHz spectrometer equipped with an actively *z*-gradient shielded triple resonance probe.

Crystallography

Crystallization of the native AnkR_AS/AnkB_repeats complex and its SeMet derivative, and the Nav1.2_ABD-C/AnkB_repeats_R1-9 complex were performed using the hanging drop vapour diffusion method at 16 ºC. Crystals of the ANK repeats/AS complex were obtained from the crystallization buffer containing 0.5 M ammonium sulfate, 1.0 M lithium sulfate, and 0.1 M sodium citrate at pH 5.6. Crystals of the Nav1.2_ABD-C/AnkB_repeats_R1-9 complex was harvested in the crystallization condition with 1.8 M ammonium sulfate, 6-8% dioxane, and 0.1 M MES pH 6.5. Before diffraction experiments, crystals were soaked in crystallization solution containing 30% glycerol for cryoprotection. The diffraction data were

collected at Shanghai Synchrotron Radiation Facility and processed and scaled using HKL2000 (Otwinowski and Minor, 1997) (Table 1).

By using the single isomorphous replacement with anomalous scattering method, the Se-Met sites were found and refined, and the initial phase was determined in AutoSHARP (Vonrhein et al., 2007). The structure model of ANK repeats was built manually based on the experimental phase and the last 12 ANK repeats of AnkR_repeats (PBD id: 1N11) (Michaely et al., 2002). Since the AS peptide contains three Met residues, the building of the AS structure was guided by the Se-anomalous difference map as the reference (Figure 2-figure supplement 2). Each asymmetric unit contains one ANK repeats/AS molecule. The model was refined against the Se-Met dataset of ANK repeats/AS in PHENIX (Adams et al., 2002). COOT (Emsley and Cowtan, 2004) was used for model rebuilding and adjustments. In the final stage, an additional TLS refinement was performed in PHENIX. The initial phase of the Nav1.2_ABD-C/AnkB_repeats_R1-9 complex was determined by molecular replacement using the different repeat regions of the ANK repeats structure as the search models. The Nav1.2_ABD-C peptide was further built into the model. The model was refined using the same strategy as that used for ANK repeats/AS. The model qualities were check by MolProbity (Davis et al., 2007). The final refinement statistics are listed in Table 1. All structure figures were prepared by PyMOL (http://www.pymol.org/).

Hippocampal neuronal cultures

The assay was performed as previously described (He et al., 2012). The shRNA of AnkG was cloned into a BFP-pll3.7 vector with the sequence of GCGTCTCCTATTAGATCTTTC, targeting a serine-rich region shared by both the 270-kDa and 480-kDa isoforms of mouse AnkG but not the rescuing rat AnkG. Hippocampal neurons were obtained from new born C57bl/6 mice and cultured until day 4 before co-transfected with the shRNA and different forms of rescue vectors containing rat AnkG using Lipofectamine 2000. On day 7, the neurons were fixed and

processed for immunostaining. All the antibodies used in the study were the same as those described in the previous study (He et al., 2012).

Microscopy and data analysis

All the images in this study were captured using a Zeiss LSM 780 laser-scanning confocal microscope. The hippocampal neurons were captured using a 40×1.4 oil objective with 0.3-micron Z spacing and pinhole setting to 1 Airy unit. Fluorescence intensity analyses were processed using the ImageJ software. The intensity ratios in neurons were quantified and analyzed using GraphPad Prism 5. For the statistical analysis, the neuronal data were compared using one-way ANOVA followed by a Tukey post hoc test.

Author Contributions

C.W., Z.W., and M.Z. designed the experiments. C.W. performed the bulk biochemical experiments in M.Z.'s lab, and cellular assays in V.B.'s lab. Z.W. solved and analyzed the crystal structures. K.C. and C.Y. helped with the biochemical experiments and F.Y. performed the NMR assay. All authors contributed to data analysis. C.W., Z.W., V.B. and M.Z. contributed and wrote the manuscript. M.Z. coordinated the study.

Author Information

Atomic coordinates and structure factors have been deposited in the Protein Data Bank. The PDB code of ANK repeats/AnkR_AS complex is 4RLV. The PDB code of Nav1.2_ABD-C/ANK_repeats_R1-9 is 4RLY. The authors declare no competing financial interests. Correspondence and requests for materials should be addressed to M.Z. (mzhang@ust.hk).

Competing interests statement

The authors declare that on competing interests exist.

Acknowledgments

We thank the Shanghai Synchrotron Radiation Facility (SSRF) BL17U for X-ray beam time, M. He, P. Jenkins and K. Walder for helping with cellular assays, and all members of the MZ and VB labs for valuable discussions. This work was supported by grants from RGC of Hong Kong to MZ (663811, 663812, 664113, HKUST6/CRF/10, SEG_HKUST06, AoE/M09/12, and T13-607/12R) and the National Key Basic Research Program of China (2014CB910204 to MZ). MZ is a Kerry Holdings Professor in Science and a Senior Fellow of IAS at HKUST.

References

Abdi, K.M., Mohler, P.J., Davis, J.Q., and Bennett, V. (2005). Isoform Specificity of Ankyrin-B: A site in the divergent C-terminal domain is required for intramolecular association. J. Biol. Chem. *281*, 5741-5749.

Adams, P.D., Grosse-Kunstleve, R.W., Hung, L.W., Ioerger, T.R., McCoy, A.J., Moriarty, N.W., Read, R.J., Sacchettini, J.C., Sauter, N.K., and Terwilliger, T.C. (2002). PHENIX: building new software for automated crystallographic structure determination. Acta Crystallogr. D Biol. Crystallogr. *58*, 1948-1954.

Ango, F., di Cristo, G., Higashiyama, H., Bennett, V., Wu, P., and Huang, Z.J. (2004). Ankyrin-based subcellular gradient of neurofascin, an immunoglobulin family protein, directs GABAergic innervation at purkinje axon initial segment. Cell *119*, 257-272.

Ayalon, G., Davis, J.Q., Scotland, P.B., and Bennett, V. (2008). An Ankyrin-Based Mechanism for Functional Organization of Dystrophin and Dystroglycan. Cell *135*, 1189-1200.

Ayalon, G., Hostettler, J.D., Hoffman, J., Kizhatil, K., Davis, J.Q., and Bennett, V. (2011). Ankyrin-B Interactions with Spectrin and Dynactin-4 Are Required for Dystrophin-based Protection of Skeletal Muscle from Exercise Injury. J. Biol. Chem. *286*, 7370-7378.

Bennett, V., and Chen, L. (2001). Ankyrins and cellular targeting of diverse membrane proteins to physiological sites. Curr. Opin. Cell Biol. *13*, 61-67.

Bennett, V., and Healy, J. (2009). Membrane Domains Based on Ankyrin and Spectrin Associated with Cell-Cell Interactions. Cold Spring Harb. Perspect. Biol. *1*, a003012-a003012.

Bennett, V., and Lorenzo, D.N. (2013). Spectrin- and ankyrin-based membrane domains and the evolution of vertebrates. Curr. Top. Membr. *72*, 1-37.

Bennett, V., and Stenbuck, P.J. (1979a). Identification and partial purification of ankyrin, the high affinity membrane attachment site for human erythrocyte spectrin. J. Biol. Chem. *254*, 2533-2541.

Bennett, V., and Stenbuck, P.J. (1979b). The membrane attachment protein for

674 spectrin is associated with band 3 in human erythrocyte membranes. Nature *280*,
675 468-473.
676 Brechet, A., Fache, M.P., Brachet, A., Ferracci, G., Baude, A., Irondelle, M., Pereira,
677 S., Leterrier, C., and Dargent, B. (2008). Protein kinase CK2 contributes to the
678 organization of sodium channels in axonal membranes by regulating their interactions
679 with ankyrin G. J. Cell Biol. *183*, 1101-1114.
680 Cai, X., and Zhang, Y. (2006). Molecular evolution of the ankyrin gene family. Mol.
681 Biol. Evol. *23*, 550-558.
682 Chook, Y.M., and Blobel, G. (2001). Karyopherins and nuclear import. Curr. Opin.
683 Struct. Biol. *11*, 703-715.
684 Conti, E., Uy, M., Leighton, L., Blobel, G., and Kuriyan, J. (1998). Crystallographic
685 analysis of the recognition of a nuclear localization signal by the nuclear import factor
686 karyopherin alpha. Cell *94*, 193-204.
687 Cunha, S.R., Hund, T.J., Hashemi, S., Voigt, N., Li, N., Wright, P., Koval, O., Li, J.,
688 Gudmundsson, H., Gumina, R.J., *et al.* (2011). Defects in Ankyrin-Based Membrane
689 Protein Targeting Pathways Underlie Atrial Fibrillation. Circulation *124*, 1212-1222.
690 Davis, I.W., Leaver-Fay, A., Chen, V.B., Block, J.N., Kapral, G.J., Wang, X., Murray,
691 L.W., Arendall, W.B., 3rd, Snoeyink, J., Richardson, J.S., *et al.* (2007). MolProbity:
692 all-atom contacts and structure validation for proteins and nucleic acids. Nucleic
693 Acids Res. *35*, W375-383.
694 Davis, L.H., Davis, J.Q., and Bennett, V. (1992). Ankyrin regulation: an alternatively
695 spliced segment of the regulatory domain functions as an intramolecular modulator. J.
696 Biol. Chem. *267*, 18966-18972.
697 Dedman, A., McQuillin, A., Kandaswamy, R., Sharp, S., Anjorin, A., and Gurling, H.
698 (2012). Sequencing of the ANKYRIN 3 gene (ANK3) encoding ankyrin G in bipolar
699 disorder reveals a non-conservative amino acid change in a short isoform of ankyrin
700 G. Am. J. Med Genet. B, Neuropsychiatr. Genet. *159B*, 328-335.
701 Emsley, P., and Cowtan, K. (2004). Coot: model-building tools for molecular graphics.
702 Acta Crystallogr. D Biol. Crystallogr. *60*, 2126-2132.
703 Fache, M.P., Moussif, A., Fernandes, F., Giraud, P., Garrido, J.J., and Dargent, B.

(2004). Endocytotic elimination and domain-selective tethering constitute a potential mechanism of protein segregation at the axonal initial segment. J. Cell Biol. *166*, 571-578.

Ferreira, M.A., O'Donovan, M.C., Meng, Y.A., Jones, I.R., Ruderfer, D.M., Jones, L., Fan, J., Kirov, G., Perlis, R.H., Green, E.K., *et al.* (2008). Collaborative genome-wide association analysis supports a role for ANK3 and CACNA1C in bipolar disorder. Nat. Genet. *40*, 1056-1058.

Galiano, M.R., Jha, S., Ho, T.S., Zhang, C., Ogawa, Y., Chang, K.J., Stankewich, M.C., Mohler, P.J., and Rasband, M.N. (2012). A Distal Axonal Cytoskeleton Forms an Intra-Axonal Boundary that Controls Axon Initial Segment Assembly. Cell *149*, 1125-1139.

Gallagher, P.G. (2005). Hematologically important mutations: ankyrin variants in hereditary spherocytosis. Blood Cells Mol. Dis. *35*, 345-347.

Garrido, J.J., Giraud, P., Carlier, E., Fernandes, F., Moussif, A., Fache, M.P., Debanne, D., and Dargent, B. (2003). A Targeting Motif Involved in Sodium Channel Clustering at the Axonal Initial Segment. Science *300*, 2091-2094.

Garver, T.D., Ren, Q., Tuvia, S., and Bennett, V. (1997). Tyrosine phosphorylation at a site highly conserved in the L1 family of cell adhesion molecules abolishes ankyrin binding and increases lateral mobility of neurofascin. J. Cell Biol. *137*, 703-714.

Gasser, A., Ho, T.S., Cheng, X., Chang, K.J., Waxman, S.G., Rasband, M.N., and Dib-Hajj, S.D. (2012). An AnkyrinG-Binding Motif Is Necessary and Sufficient for Targeting Nav1.6 Sodium Channels to Axon Initial Segments and Nodes of Ranvier. J. Neurosci. *32*, 7232-7243.

Graham, T.A., Weaver, C., Mao, F., Kimelman, D., and Xu, W. (2000). Crystal structure of a beta-catenin/Tcf complex. Cell *103*, 885-896.

Grubb, M.S., and Burrone, J. (2010). Activity-dependent relocation of the axon initial segment fine-tunes neuronal excitability. Nature *465*, 1070-1074.

Gutzmann, A., Ergul, N., Grossmann, R., Schultz, C., Wahle, P., and Engelhardt, M. (2014). A period of structural plasticity at the axon initial segment in developing visual cortex. Front. Neuroanat. *8*, 11.

734 Hashemi, S.M., Hund, T.J., and Mohler, P.J. (2009). Cardiac ankyrins in health and
735 disease. J. Mol. Cell. Cardiol. *47*, 203-209.
736 He, M., Jenkins, P., and Bennett, V. (2012). Cysteine 70 of ankyrin-g is
737 s-palmitoylated and is required for function of ankyrin-g in membrane domain
738 assembly. J. Biol. Chem. *287*, 43995-44005.
739 He, M., Tseng, W.C., and Bennett, V. (2013). A single divergent exon inhibits
740 ankyrin-B association with the plasma membrane. J. Biol. Chem. *288*, 14769-14779.
741 Hedstrom, K.L., Ogawa, Y., and Rasband, M.N. (2008). AnkyrinG is required for
742 maintenance of the axon initial segment and neuronal polarity. J. Cell Biol. *183*,
743 635-640.
744 Hedstrom, K.L., Xu, X., Ogawa, Y., Frischknecht, R., Seidenbecher, C.I., Shrager, P.,
745 and Rasband, M.N. (2007). Neurofascin assembles a specialized extracellular matrix
746 at the axon initial segment. J. Cell Biol. *178*, 875-886.
747 Hill, A.S., Nishino, A., Nakajo, K., Zhang, G., Fineman, J.R., Selzer, M.E., Okamura,
748 Y., and Cooper, E.C. (2008). Ion channel clustering at the axon initial segment and
749 node of Ranvier evolved sequentially in early chordates. PLoS Genet. *4*, e1000317.
750 Howard, J., and Bechstedt, S. (2004). Hypothesis: a helix of ankyrin repeats of the
751 NOMPC-TRP ion channel is the gating spring of mechanoreceptors. Curr. Biol. *14*,
752 R224-226.
753 Hu, W., Tian, C., Li, T., Yang, M., Hou, H., and Shu, Y. (2009). Distinct contributions
754 of Nav1.6 and Nav1.2 in action potential initiation and backpropagation. Nat.
755 Neurosci. *12*, 996-1002.
756 Huber, A.H., and Weis, W.I. (2001). The structure of the beta-catenin/E-cadherin
757 complex and the molecular basis of diverse ligand recognition by beta-catenin. Cell
758 *105*, 391-402.
759 Hund, T.J., Wright, P.J., Dun, W., Snyder, J.S., Boyden, P.A., and Mohler, P.J. (2008).
760 Regulation of the ankyrin-B-based targeting pathway following myocardial infarction.
761 Cardiovasc. Res. *81*, 742-749.
762 Iqbal, Z., Vandeweyer, G., van der Voet, M., Waryah, A.M., Zahoor, M.Y., Besseling,
763 J.A., Roca, L.T., Vulto-van Silfhout, A.T., Nijhof, B., Kramer, J.M., *et al.* (2013).

764 Homozygous and heterozygous disruptions of ANK3: at the crossroads of
765 neurodevelopmental and psychiatric disorders. Hum. Mol. Genet. *22*, 1960-1970.
766 Jenkins, S.M., and Bennett, V. (2001). Ankyrin-G coordinates assembly of the
767 spectrin-based membrane skeleton, voltage-gated sodium channels, and L1 CAMs at
768 Purkinje neuron initial segments. J. Cell Biol. *155*, 739-746.
769 Kobe, B. (1999). Autoinhibition by an internal nuclear localization signal revealed by
770 the crystal structure of mammalian importin alpha. Nature structural biology *6*,
771 388-397.
772 Kole, M.H., Ilschner, S.U., Kampa, B.M., Williams, S.R., Ruben, P.C., and Stuart, G.J.
773 (2008). Action potential generation requires a high sodium channel density in the
774 axon initial segment. Nat. Neurosci. *11*, 178-186.
775 Kole, M.H., and Stuart, G.J. (2012). Signal processing in the axon initial segment.
776 Neuron *73*, 235-247.
777 Kuba, H., Oichi, Y., and Ohmori, H. (2010). Presynaptic activity regulates Na(+)
778 channel distribution at the axon initial segment. Nature *465*, 1075-1078.
779 Le Bras, B., Freal, A., Czarnecki, A., Legendre, P., Bullier, E., Komada, M., Brophy,
780 P.J., Davenne, M., and Couraud, F. (2013). In vivo assembly of the axon initial
781 segment in motor neurons. Brain Struct. Funct.
782 Le Scouarnec, S., Bhasin, N., Vieyres, C., Hund, T.J., Cunha, S.R., Koval, O.,
783 Marionneau, C., Chen, B., Wu, Y., Demolombe, S., *et al.* (2008). Dysfunction in
784 ankyrin-B-dependent ion channel and transporter targeting causes human sinus node
785 disease. Proc. Natl Acad. Sci. USA *105*, 15617-15622.
786 Lee, G., Abdi, K., Jiang, Y., Michaely, P., Bennett, V., and Marszalek, P.E. (2006).
787 Nanospring behaviour of ankyrin repeats. Nature *440*, 246-249.
788 Lemaillet, G., Walker, B., and Lambert, S. (2003). Identification of a Conserved
789 Ankyrin-binding Motif in the Family of Sodium Channel α Subunits. J. Biol. Chem.
790 *278*, 27333-27339.
791 Li, J., Mahajan, A., and Tsai, M.-D. (2006). Ankyrin Repeat: A Unique Motif
792 Mediating Protein−Protein Interactions. Biochemistry *45*, 15168-15178.
793 Lowe, J.S., Palygin, O., Bhasin, N., Hund, T.J., Boyden, P.A., Shibata, E., Anderson,

M.E., and Mohler, P.J. (2008). Voltage-gated Nav channel targeting in the heart requires an ankyrin-G dependent cellular pathway. J. Cell Biol. *180*, 173-186.

Michaely, P., Tomchick, D.R., Machius, M., and Anderson, R.G. (2002). Crystal structure of a 12 ANK repeat stack from human ankyrinR. EMBO J. *21*, 6387-6396.

Mohler, P.J., Davis, J.Q., and Bennett, V. (2005). Ankyrin-B coordinates the Na/K ATPase, Na/Ca exchanger, and InsP3 receptor in a cardiac T-tubule/SR microdomain. PLoS Biol. *3*, e423.

Mohler, P.J., Gramolini, A.O., and Bennett, V. (2002). The Ankyrin-B C-terminal domain determines activity of Ankyrin-B/G chimeras in rescue of abnormal inositol 1,4,5-trisphosphate and ryanodine receptor distribution in Ankyrin-B (-/-) neonatal cardiomyocytes. J. Biol. Chem. *277*, 10599-10607.

Mohler, P.J., Le Scouarnec, S., Denjoy, I., Lowe, J.S., Guicheney, P., Caron, L., Driskell, I.M., Schott, J.J., Norris, K., Leenhardt, A., *et al.* (2007). Defining the Cellular Phenotype of "Ankyrin-B Syndrome" Variants: Human ANK2 Variants Associated With Clinical Phenotypes Display a Spectrum of Activities in Cardiomyocytes. Circulation *115*, 432-441.

Mohler, P.J., Rivolta, I., Napolitano, C., Lemaillet, G., Lambert, S., Priori, S.G., and Bennett, V. (2004). Nav1.5 E1053K mutation causing Brugada syndrome blocks binding to ankyrin-G and expression of Nav1.5 on the surface of cardiomyocytes. Proc. Natl Acad. Sci. USA *101*, 17533-17538.

Mohler, P.J., Schott, J.J., Gramolini, A.O., Dilly, K.W., Guatimosim, S., duBell, W.H., Song, L., Haurogné, K., Kyndt, F., Ali, M.E., *et al.* (2003). Ankyrin-B mutation causes type 4 long-QT cardiac arrhythmia and sudden cardiac death. Nature *421*, 634-639.

Otwinowski, Z., and Minor, W. (1997). Processing of X-ray Diffraction Data Collected in Oscillation Mode. Methods Enzymol. *276*, 307-326.

Pan, Z., Kao, T., Horvath, Z., Lemos, J., Sul, J.-Y., Cranstoun, S.D., Bennett, V., Scherer, S.S., and Cooper, E.C. (2006). A Common Ankyrin-G-Based Mechanism Retains KCNQ and NaV Channels at Electrically Active Domains of the Axon. J. Neurosci. *26*, 2599-2613.

824 Rasband, M.N. (2010). The axon initial segment and the maintenance of neuronal
825 polarity. Nat. Rev. Neurosci. *11*, 552-562.
826 Rueckert, E.H., Barker, D., Ruderfer, D., Bergen, S.E., O'Dushlaine, C., Luce, C.J.,
827 Sheridan, S.D., Theriault, K.M., Chambert, K., Moran, J., *et al.* (2013). Cis-acting
828 regulation of brain-specific ANK3 gene expression by a genetic variant associated
829 with bipolar disorder. Mol. Psychiatry *18*, 922-929.
830 Shi, L., Zhang, X., Golhar, R., Otieno, F.G., He, M., Hou, C., Kim, C., Keating, B.,
831 Lyon, G.J., Wang, K., *et al.* (2013). Whole-genome sequencing in an autism multiplex
832 family. Mol. Autism *4*, 8.
833 Sobotzik, J.M., Sie, J.M., Politi, C., Del Turco, D., Bennett, V., Deller, T., and Schultz,
834 C. (2009). AnkyrinG is required to maintain axo-dendritic polarity in vivo. Proc. Natl
835 Acad. Sci. USA *106*, 17564-17569.
836 Tamaskovic, R., Simon, M., Stefan, N., Schwill, M., and Pluckthun, A. (2012).
837 Designed ankyrin repeat proteins (DARPins) from research to therapy. Methods
838 Enzymol. *503*, 101-134.
839 Vonrhein, C., Blanc, E., Roversi, P., and Bricogne, G. (2007). Automated structure
840 solution with autoSHARP. Methods Mol. Biol. *364*, 215-230.
841 Wang, C., Yu, C., Ye, F., Wei, Z., and Zhang, M. (2012). Structure of the
842 ZU5-ZU5-UPA-DD tandem of ankyrin-B reveals interaction surfaces necessary for
843 ankyrin function. Proc. Natl Acad. Sci. USA *109*, 4822-4827.
844 Whittard, J.D., Sakurai, T., Cassella, M.R., Gazdoiu, M., and Felsenfeld, D.P. (2006).
845 MAP kinase pathway-dependent phosphorylation of the L1-CAM ankyrin binding site
846 regulates neuronal growth. Mol. Biol. Cell *17*, 2696-2706.
847 Xu, C., Jin, J., Bian, C., Lam, R., Tian, R., Weist, R., You, L., Nie, J., Bochkarev, A.,
848 Tempel, W., *et al.* (2012). Sequence-specific recognition of a PxLPxI/L motif by an
849 ankyrin repeat tumbler lock. Sci. Signal. *5*, ra39.
850 Xu, D., Farmer, A., and Chook, Y.M. (2010). Recognition of nuclear targeting signals
851 by Karyopherin-beta proteins. Curr. Opin. Struct. Biol. *20*, 782-790.
852 Zhou, D., Lambert, S., Malen, P.L., Carpenter, S., Boland, L.M., and Bennett, V.
853 (1998). AnkyrinG is required for clustering of voltage-gated Na channels at axon

initial segments and for normal action potential firing. J. Cell Biol. *143*, 1295-1304.

Zhu, J., Wen, W., Zheng, Z., Shang, Y., Wei, Z., Xiao, Z., Pan, Z., Du, Q., Wang, W., and Zhang, M. (2011). LGN/mInsc and LGN/NuMA complex structures suggest distinct functions in asymmetric cell division for the Par3/mInsc/LGN and Galphai/LGN/NuMA pathways. Mol. Cell *43*, 418-431.

Zonta, B., Desmazieres, A., Rinaldi, A., Tait, S., Sherman, D.L., Nolan, M.F., and Brophy, P.J. (2011). A critical role for Neurofascin in regulating action potential initiation through maintenance of the axon initial segment. Neuron *69*, 945-956.

Figure 1. Identification of a 48-residue auto-inhibitory segment that binds to ANK repeats.

(A) Schematic diagrams showing the domain organization of ankyrins. The AnkR-specific auto-inhibitory segment (AS) is indicated within the C-terminal regulatory domain. The same color codes (24 ANK repeats in rainbow and the AnkR_AS in magenta) are used throughout the paper unless otherwise stated.

(B) ITC-based mapping of the minimal AnkR_repeats binding region in the C-terminal regulatory domain. The minimal and complete auto-inhibitory segment identified is highlighted in magenta. "ND" denotes that these constructs had no detectable binding to ANK repeats.

(C) ITC-derived binding curve of AnkR_AS titrated to AnkR_repeats.

(D) The binding affinities between AS and ANK repeats of the three ankyrin isoforms.

Figure 2. Vertebrate ANK repeats of ankyrins share the same architecture and target binding properties.

(A) Sequence alignment of the 24 ANK repeats of human AnkB. Similar and identical residues are labeled grey and black, respectively. The helix formation residues are boxed with corresponding colors. The hydrophobic residues selected for mutation studies described in Figure 3 and onwards are labeled with corresponding colors. The last nine amino acids labeled in red from R24 are used as the C-terminal capping sequence for designed truncation mutants of various lengths of ANK repeats used in this study.

(B) Sequence conservation map of the 24 ANK repeats of vertebrate ankyrins. The conservation score for each residue is calculated based on the sequences of vertebrate ankyrins aligned in Figure 2-figure supplement 3 through the Scorecons server (http://www.ebi.ac.uk/thornton-srv/databases/cgi-bin/valdar/scorecons_server.pl). The position of each residue is the same that as shown in panel A.

(C) Overall structure of the ANK repeats/AS complex viewed from the top (left) and side (right). The three AS-binding surfaces on ANK repeats are circled by black dashed ovals. The sequences of AnkR_AS are listed below.

(D) Surface conservation map of ANK repeats viewed from the side. The conservation map is derived from the ankyrins from worm to human as shown in Figure 2-figure supplement 3 with the same color coding scheme as in panel (B).

Figure 2-figure supplement 1. The fusion of AnkR_AS to the N-terminus AnkB_repeats does not alter the conformation of the ANK repeats/AS complex.

(A) ^{1}H-^{13}C HSQC spectrum showing the $^{13}CH_3$-Met-labeled, covalently-linked AnkR_AS-AnkB_repeats fusion protein. The resolved Met methyl groups are labeled with blue asterisks.

(B) Superposition plot of the ^{1}H-^{13}C HSQC spectra of the covalently-linked (red) and thrombin-cleaved ANK repeats/AS complex, showing that the two spectra are essentially identical. The data also indicate that the fusion of AS to the N-terminal of ANK repeats, a step necessary for obtaining crystals of the complex, does not alter the conformation of the complex.

Figure 2-figure supplement 2. Crystallographic characterization of the ANK repeats/AS structure.

(A) Electron density (2Fo-Fc) map of ANK repeats/AS superimposed on the C_α-model. The map is contoured at 1.5σ. Insert, the Se-anomalous difference map contoured at 4σ shows four Se-peaks around R7-9 of the ANK repeats, indicating that three Met residues (Met1601, Met1604, and Met1607) of AnkR_AS are located at the site-2 of the ANK repeats, which also contains a Met (Met338).

(B) The 2Fo-Fc map of AnkR_AS contoured at 1σ with the final structural model superimposed. The densities of three selected side-chain interactions from the AS and ANK repeats are shown in the inserts.

Figure 2-figure supplement 3. Amino acid sequence alignment of ANK repeats of ankyrins. In this alignment, residues that are absolutely conserved and highly conserved are highlighted in red and yellow, respectively. The secondary structural elements are indicated above the alignment. The interface residues at the site-1, 2, and 3 for the binding of the ANK repeats to AnkR_AS are labeled by number '1', '2', and '3', respectively. The interface residues that involved in the ANK repeats/Nav1.2_ABD-C interaction are marked by triangles. The vertebrate ankyrin ANK repeats are aligned together, and used to derive the ANK repeats conservation plot shown in Figure 2B.

Video 1. Surface conservation of 24 ANK repeats. This video shows the concave groove is highly conserved across various species from human to worms.

Figure 3. Structural and biochemical characterizations of target binding properties of ANK repeats.

(A-C) Stereo views showing the detailed ANK repeats/AS interfaces of the three binding sites shown in Figure 1E. Hydrogen bonds and salt bridges are indicated by dashed lines.

(D) Cartoon-diagram of the first 14 repeats of the 24 ANK repeats. Different truncations used for the biochemical analyses are indicated below. Mutations of hydrophobic residues in the three AS binding sites are labeled. Red stars indicate the locations of the mutation sites.

(E) Example ITC curves showing the bindings of Nav1.2_ABD or Nfasc_ABD to the wild-type or mutant ANK repeats.

(F) The dissociation constants of the binding reactions of various mutants of ANK repeats to Nav1.2 and Nfasc derived from the ITC-based assays.

Figure 3-figure supplement 1. Analytical gel filtration analyses showing that binding of AS to AnkG_repeats prevents Nav1.2 and Nfasc ABDs from binding to AnkG_repeats.

The AS was fused to the N-terminus of AnkG_repeats. No complex peaks formed between the fusion protein and Nav1.2 ABD (A) or Nfasc ABD (B), as the mixture of the two proteins in each experiment did not change their elution volumes compared to that of each isolated protein. For clarity, the curve of the mixture in (B) was up-shifted by 10 mAU.

Figure 3-figure supplement 2. ITC-based analyses of the AnkG_repeats/Nfasc_ABD interaction.

(A) Schematic diagram showing the domain organization of the L1-family cell adhesion molecules (L1CAMs). The amino acid numbers labeled is corresponding to mouse Nfasc used in this study.

(B) ITC titration of ABD (1187-1214) to AnkG_repeats.

(C) ITC titration of the entire cytoplasmic tail (1132-1240) to AnkG_repeats, showing that the segment corresponding to 1187-1214 encompasses the complete binding domain for AnkG_repeats.

Figure 3-figure supplement 3. The ITC curves of the bindings of various ANK repeats to Nav1.2_ABD. The proteins assayed in each experiment are labeled on each panel with cartoon drawing. The curves were used to derive the dissociation constants shown in Figure 3F.

Figure 3-figure supplement 4. The ITC curves of the bindings of various ANK repeats to Nfasc_ABD. The proteins assayed in each experiment are labeled on each panel with cartoon drawing. The curves were used to derive the dissociation constants shown in Figure 3F.

Figure 4. Fluorescence polarization-based measurement of the binding affinities of different targets to AnkB_repeats WT and its mutants.

(A) Fluorescence polarization-based measurement of the binding affinities of AnkR_AS peptide to AnkB_repeats WT and its mutants. The insert shows the

expanded view of the binding curves of the AnkR_AS peptides to WT and LFL of AnkB_repeats. The binding affinity between AnkR_AS and AnkB_repeats WT measured through this experiment is slightly different from the ITC assay (0.14 μM vs 0.40 μM). This may come from the different measuring system, but the overall affinity range is quite similar.

(B) Fluorescence polarization-based measurement of the binding affinities of the KCNQ2 peptide to AnkB_repeats WT and its various mutants.

(C) Fluorescence polarization-based measurement of the binding affinities of the Cav1.3 peptide to AnkB_repeats and its various mutants.

The fitted binding affinities are shown within corresponding figures.

Figure 5. Characterization of the interaction between Nav1.2 and AnkG_repeats.

(A) Schematic diagram showing the domain organization of the Nav1 family ion channels. The ABD is located within the loop 2 linking the transmembrane helices II&III and separated into N- and C- parts according to the data below.

(B) Table summarizing the ITC-derived affinities of the bindings of various loop 2 fragments to AnkG_repeats.

(C) ITC curves of the bindings of Nav1.2_ABD* (upper left), ABD-N (upper right), and ABD-C (lower left) to ANK repeats, and Nav1.2_ABD-C binding to ANK repeats R1-6 (lower right), showing that ABD-C binds to the site-1 of AnkG_repeats.

(D) Amino acid sequence alignment of the ankyrin binding domains (ABD) of members of the voltage-gated sodium channel α-subunits (Nav1) family. The mouse Nav1.2 used in this study was aligned with the human family members. Residues that are absolutely conserved and highly conserved are highlighted in red and yellow, respectively. The critical Glu1112 for the binding of Nav1.2 to the ANK repeats is indicated with a star. Other residues participate in the binding with the ANK repeats are indicated by triangles. The residues responsible for binding to the site-1 of AnkG_repeats are completely conserved in all members of the Nav1 family, indicating that all sodium channels can bind to ankyrins following the mode revealed in this study.

Figure 6. The site-1 of ANK repeats is a common binding site for Nav1.2 and other targets.

(A) Ribbon representation of the binding of Nav1.2_ABD-C (light green) to the site-1 of ANK repeats (cyan). The interface residues are shown in the stick mode. Hydrogen bonds and salt bridges are indicated by dashed lines. The negatively charged Glu1112, critical for interacting with a positively charged surface formed by ANK repeats R2 and R3, is highlighted with a red box.

(B) Charge potential surface of the site-1 on the ANK repeats reveals a positively charged pocket important for anchoring of Glu1112 through charge complementation. The hydrophobic groove and the interacting residues from Nav1.2 are also shown. The surface diagram is drawn with the same orientation as in panel A. The electrostatic surface potentials were calculated by the APBS module embedded in PyMol with the nonlinear Poisson–Boltzmann equation and contoured at ± 5 kT/e.

(C) Amino acid sequence alignment of the site-1 binding sequences in various partners showing the similar sequence pattern, with the anchoring Glu boxed. The residues participating in the site-1 binding are indicated by triangles.

(D) Summary of the ITC-derived K_d values showing that Glu1112 is essential for the ANK repeats/Nav1.2 interaction.

(E) Structural comparison of the ANK repeats site-1 bindings of AnkR_AS and Nav1.2_ABD-C showing that the two targets bind to ANK repeats with essentially the same mode. Subtle conformational differences in the finger loops R4 and R5 are indicated by arrows.

Figure 6-figure supplement 1. Crystallographic characterization of the ANK repeats/Nav1.2 structure.

Electron density map of the AnkB/Nav1.2 complex contoured at 1σ with the final structural model superimposed is shown. The Nav1.2 peptide is shown as the stick model and the AnkB_repeats is shown as the Cα-model.

Figure 7. Mutations of residues at the target binding groove affect 270-kDa AnkG's function at AIS in neurons.

(A) WT 270-kDa AnkG-GFP effectively rescues AnkG self-clustering and clustering of sodium channels at AIS. The FF mutant of AnkG is clustered at AIS, but fails to rescue sodium channel clustering at AIS. BFP marks the shRNA transfected neurons (scale bars 50 μm). White boxes mark the axon initial segment, which is shown at higher magnification below each image (scale bars, 10 μm).

(B) Same as in panel A except that red signals represent anti-neurofascin staining.

(C) Quantification of anti-GFP fluorescence intensity ratio of axons to dendrites in cells depleted of endogenous 270/480-kDa AnkG and rescued with WT (n=34), FF (n=30), IL (n=24), or LF (n=24) AnkG-GFP. **, $p<0.05$. Error bars, S.E.

(D) Quantification of the anti-endogenous pan-sodium channels fluorescence intensity ratio of axons to dendrites in cells depleted of endogenous 270/480-kDa AnkG and rescued with GFP alone (n=11), WT (n=17), FF (n=16), IL (n=14) and LF (n=10) AnkG-GFP. **, $p<0.05$. Error bars, S.E.

(E) Quantification of the anti-endogenous neurofascin fluorescence intensity ratio of axons to dendrites in cells depleted of endogenous 270/480-kDa AnkG and rescued with GFP alone (n=6), WT (n=17), FF(n=14), IL (n=10) and LF (n=10) AnkG-GFP. **, $p<0.05$. Error bars, S.E.

Figure 7-figure supplement 1. The IL and LF AnkG-GFP mutants do not cluster at AIS and fail to rescue AnkG's functions in AIS.

GFP control, IL mutant of AnkG-GFP, and LF mutant of AnkG-GFP constructs were co-transfected with shRNA against mouse AnkG respectively to assay their ability in rescuing AnkG's self-clustering and clustering of sodium channels (A), and neurofascin (B) at AIS. The two AnkG-GFP mutants can neither cluster at AIS nor rescue the clustering of sodium channels or Nfasc. The quantification data are shown in Figure 7C-E.

Table 1. Statistics of data collection and model refinement

	Native ANK repeats/AS	SeMet-ANK repeats/AS	R1-9/Nav1.2_ABD-C
Data collection			
Space group	*R*32	*R*32	$P4_222$
Cell dimensions			
a, *b*, *c* (Å)	179.9, 179.9, 304.5	179.7, 179.7, 304.9	102.3, 102.3, 106.0
α, β, γ(°)	90, 90, 120	90, 90, 120	90, 90, 90
Resolution range (Å)	50 – 4.0 (4.07 – 4.0)	50 – 3.5 (3.56 – 3.5)	50 – 2.5 (2.54 – 2.5)
R_{merge} (%)[a]	8.7 (45.8)	12.1 (78.3)	7.7 (74.8)
$I/\sigma I$	17.1 (3.4)	22.5 (2.2)	29.8 (3.5)
Completeness (%)	98.9 (99.3)	96.0 (97.2)	99.4 (100)
Redundancy	4.3 (4.4)	10.2 (9.0)	9.5 (9.7)
Structure refinement			
Resolution (Å)		50 – 3.5 (3.62 – 3.5)	50 – 2.5 (2.64 – 2.5)
R_{cryst} / R_{free} (%)[b]		22.0 (35.0) / 25.3 (36.6)	18.8 (22.7) / 23.8 (24.5)
r.m.s.d bonds (Å) / angles (°)		0.013 / 1.5	0.015 / 1.5
Average B factor		113.5	63.5
No. of atoms			
protein atoms		6260	2243
water molecules		0	74
other molecules		45	57
Ramachandran plot[c]			
favored regions (%)		94.7	97.7
allowedregions(%)		5.2	2.3
outliners (%)		0.1	0.0

[a] $R_{merge} = \sum |I_i - I_m| / \sum I_i$, where I_i is the intensity of the measured reflection and I_m is the mean intensity of all symmetry related reflections.

[b] $R_{cryst} = \Sigma||F_{obs}| - |F_{calc}||/\Sigma|F_{obs}|$, where F_{obs} and F_{calc} are observed and calculated structure factors. $R_{free} = \Sigma_T||F_{obs}| - |F_{calc}||/\Sigma_T|F_{obs}|$, where T is a test data set of about 5% of the total reflections randomly chosen and set aside prior to refinement.

[c] Defined by MolProbity.

Numbers in parentheses represent the value for the highest resolution shell.

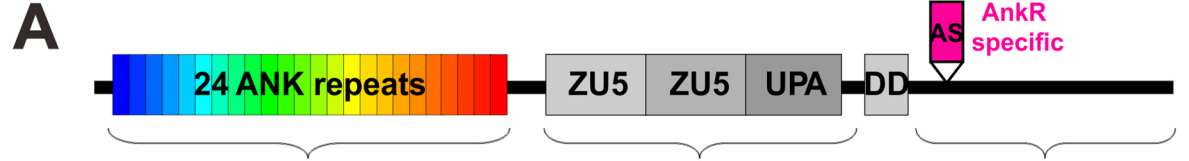

B

AnkR C-terminal regulatory domain	AnkR_repeats Kd (μM)
1529-1907	1.0 ± 0.1
1529-1825	1.0 ± 0.2
1826-1907	ND
1529-1672	1.1 ± 0.1
1673-1825	ND
1529-1600	>50
1601-1672	>50
1577-1624	0.36 ± 0.02
1577-1612	2.0 ± 0.2
1589-1624	2.2 ± 0.1
1589-1612	23 ± 15

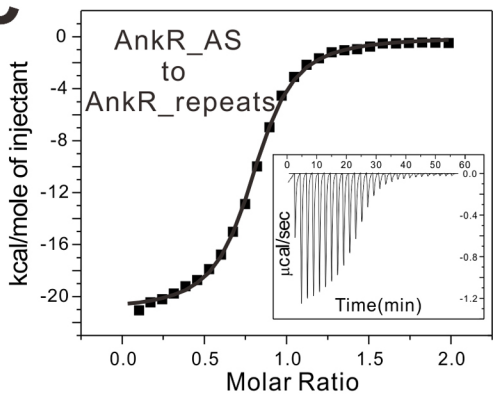

D

AnkR_AS	Kd (μM)
AnkR_repeats	0.36 ± 0.02
AnkB_repeats	0.40 ± 0.07
AnkG_repeats	0.46 ± 0.16

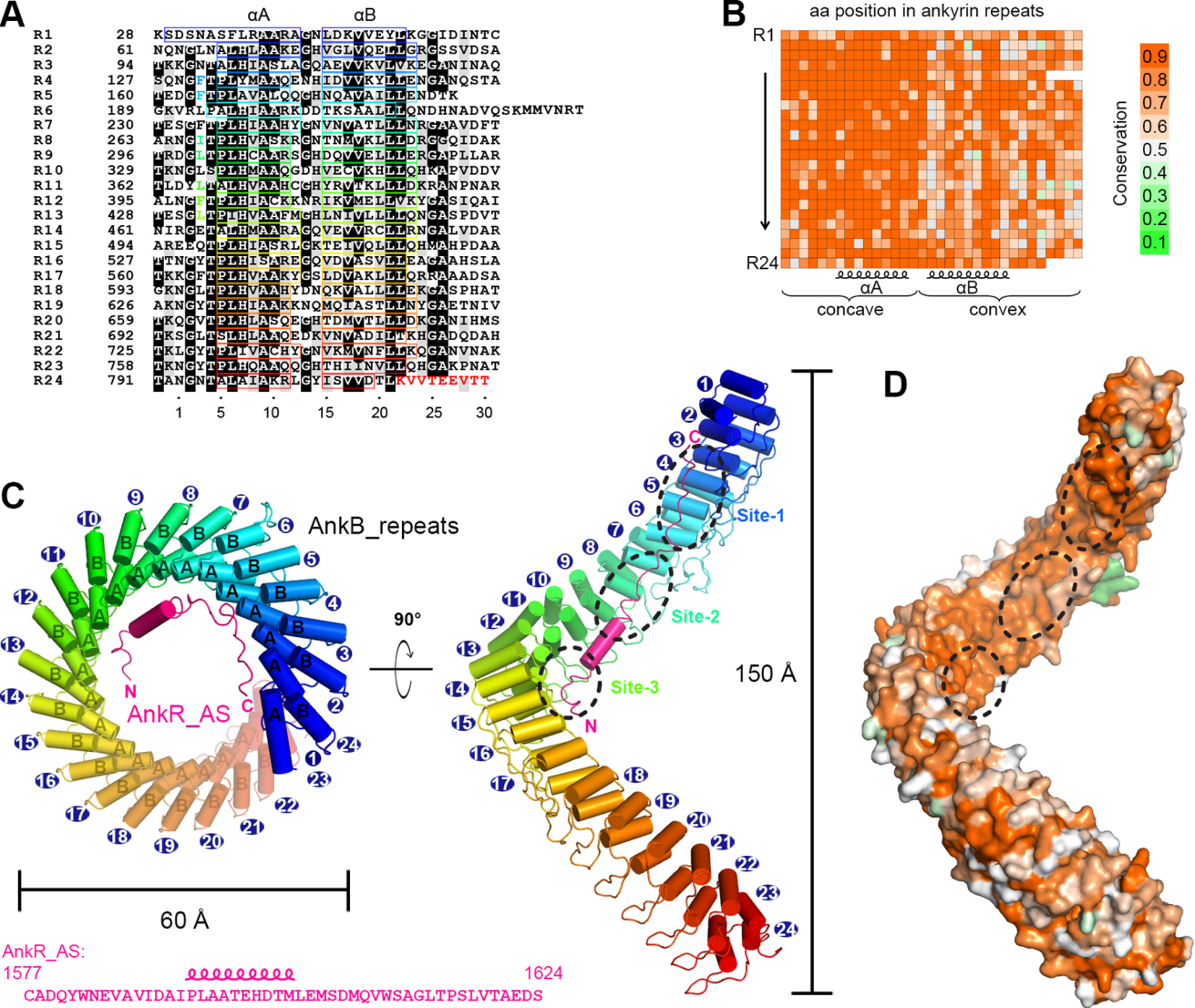
A
αA
αB
R1 28 KSDSNASFLRAARAGNLDKVVEYLKGGIDINTC
R2 61 NQNGLNALHLAAKEGHVGLVQELLGRGSSVDSA
R3 94 TKKGNTALHIASLAGQAEVVKVLVKEGANINAQ
R4 127 SQNGFTPLYMAAQENHIDVVKYLLENGANQSTA
R5 160 TEDGFTPLAVALQQGHNQAVAILLENDTK
R6 189 GKVRLPALHIAARKDDTKSAALLLQNDHNADVQSKMMVNRT
R7 230 TESGFTPLHIAAHYGNVNVATLLLNRGAAVDFT
R8 263 ARNGITPLHVASKRGNTNMVKLLLDRGGQIDAK
R9 296 TRDGLTPLHCAARSGHDQVVELLLERGAPLLAR
R10 329 TKNGLSPLHMAAQGDHVECVKHLLQHKAPVDDV
R11 362 TLDYLTALHVAAHCGHYRVVTKLLLDKRANPNAR
R12 395 ALNGFTPLHIACKKNRIKVMELLVKYGASIQAI
R13 428 TESGLTPLHVAAFMGHLNIVLLLQNGASPDVT
R14 461 NIRGETALHMAARAGQVEVVRCLLRNGALVDAR
R15 494 AREEQTPLHIASRLGKTEIVQLLLQHMAHPDAA
R16 527 TTNGYTPLHISAREGQVDVASVLLEAGAAHSLA
R17 560 TKKGFTPLHVAAKYGSLDVAKLLLQRNAAADSA
R18 593 GKNGLTPLHVAAHYDNQKVALLLLEKGASPHAT
R19 626 AKNGYTPLHIAAKKNQMQIASTLLNYGAETNIV
R20 659 TKQGVTPLHLASQEGHTDMVTLLLDKGANIHMS
R21 692 TKSGLTSLHLAAQEDKVNVADILITKHGADQDAH
R22 725 TKLGYTPLIVACHYGNVKMVNFLLKQGANVNAK
R23 758 TKNGYTPLHQAAQQGHTHIINVLLQHGAKPNAT
R24 791 TANGNTALAIAKRLGYISVVDTLKVVTEEVTT
1 5 10 15 20 25 30
B
aa position in ankyrin repeats
R1
R24
αA
αB
concave
convex
Conservation
0.9
0.8
0.7
0.6
0.5
0.4
0.3
0.2
0.1
C
AnkB_repeats
N
C
AnkR_AS
60 Å
90°
Site-1
Site-2
Site-3
150 Å
AnkR_AS:
1577
1624
CADQYWNEVAVIDAIPLAATEHDTMLEMSDMQVWSAGLTPSLVTAEDS
D

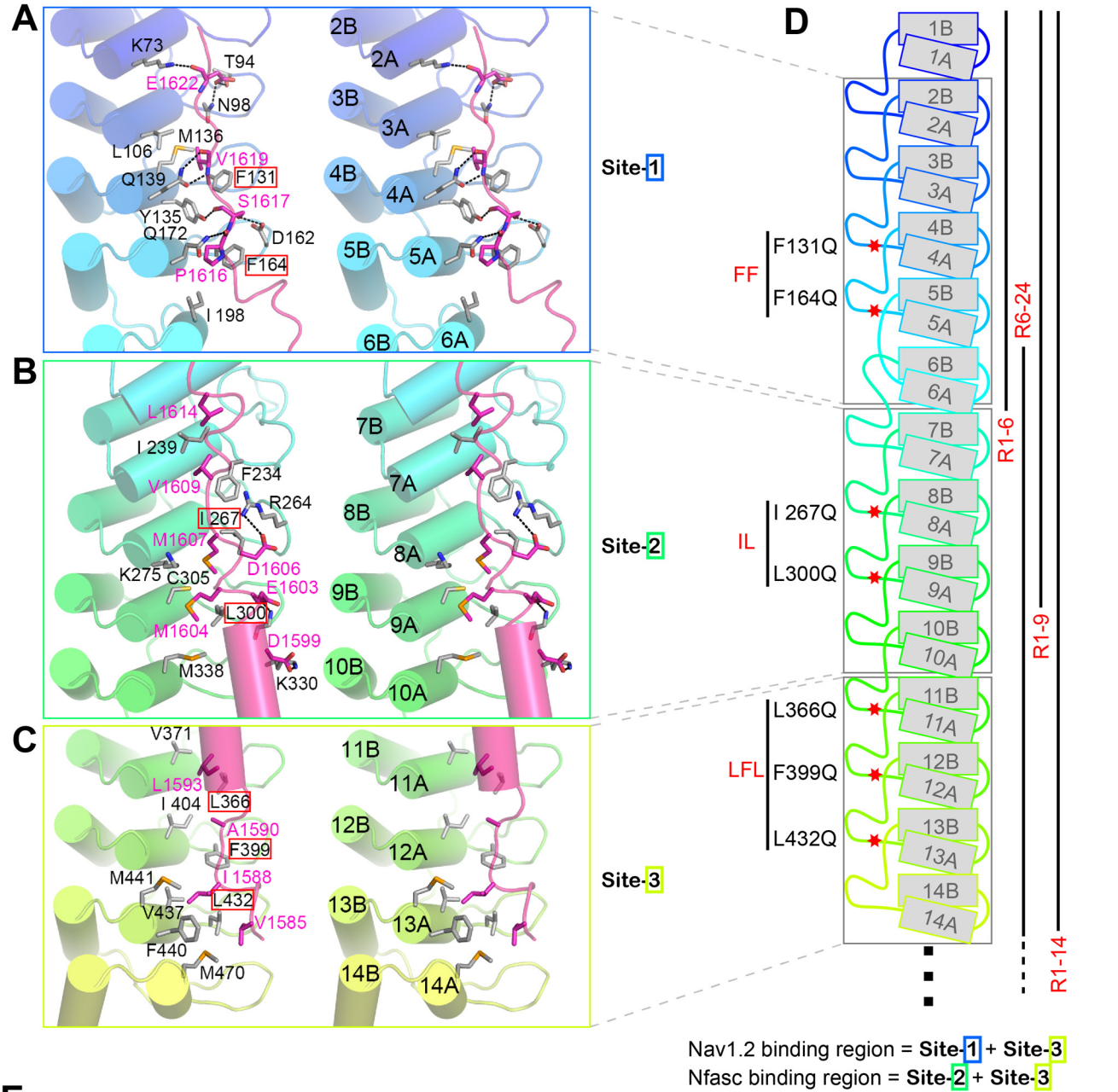

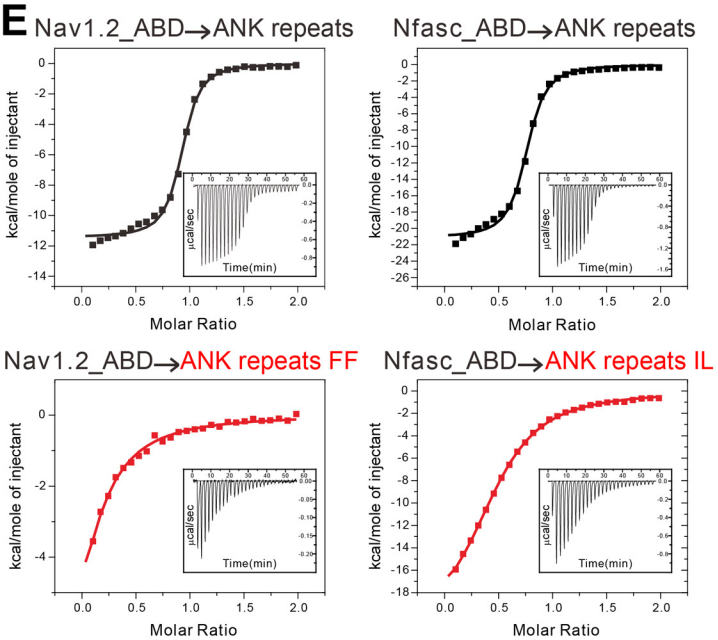

F

ANK repeats	Nav1.2_ABD Kd (μM)	Nfasc_ABD Kd (μM)
WT	0.17 ±0.01	0.21 ±0.02
FF (1)	6.6 ±0.7	0.17 ±0.02
IL (2)	0.22 ±0.02	2.8 ±0.2
LFL (3)	1.1 ±0.1	6.0 ±0.2
R1-6 (1)	2.3 ± 0.1	Not detectable
R6-24 (2 3)	Not detectable	0.14 ±0.02
R1-9 (1 2)	3.5 ± 0.2	Not detectable
R1-14 (1 2 3)	0.29 ±0.02	0.063 ±0.005

The abrrevations in red is the same as those in the panel (D).

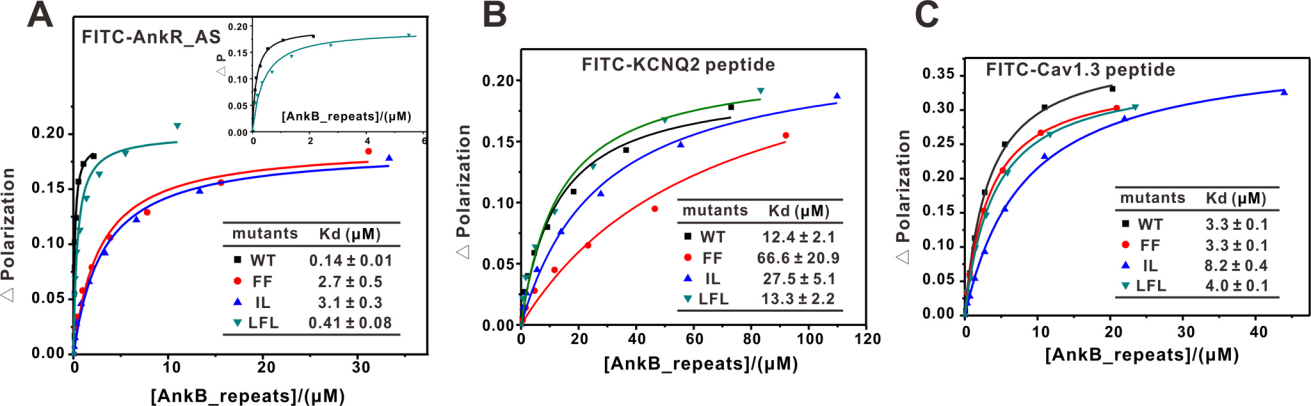
A
FITC-AnkR_AS
△ Polarization
[AnkB_repeats]/(μM)
mutants Kd (μM)
WT 0.14 ± 0.01
FF 2.7 ± 0.5
IL 3.1 ± 0.3
LFL 0.41 ± 0.08
B
FITC-KCNQ2 peptide
△ Polarization
[AnkB_repeats]/(μM)
mutants Kd (μM)
WT 12.4 ± 2.1
FF 66.6 ± 20.9
IL 27.5 ± 5.1
LFL 13.3 ± 2.2
C
FITC-Cav1.3 peptide
△ Polarization
[AnkB_repeats]/(μM)
mutants Kd (μM)
WT 3.3 ± 0.1
FF 3.3 ± 0.1
IL 8.2 ± 0.4
LFL 4.0 ± 0.1

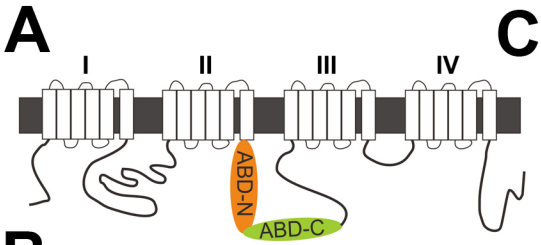

B

ANK repeats	Nav1.2	Kd(μM)
WT	ABD (1035 - 1129)	0.17 ±0.01
WT	ABD* (1035 - 1119)	0.17 ±0.01
WT	ABD-N (1035 - 1102)	8.1 ±1.1
WT	ABD-C (1103 - 1129)	2.7 ±0.1
R1-6	ABD-C (1103 - 1129)	2.3 ±0.2

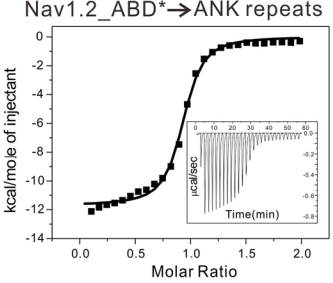

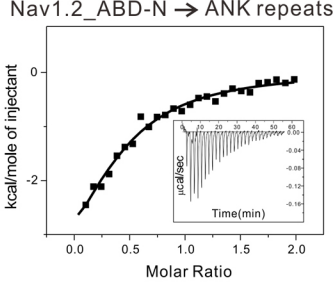

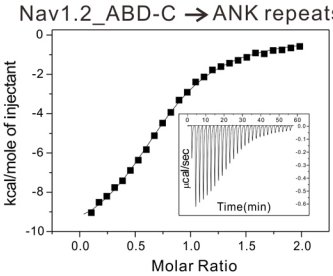

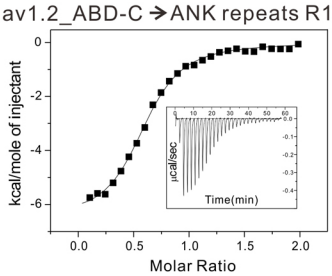

D

```
                                                ABD-N
mNav1.2  1035  KALDEIKPLEDLN.NKKDSCISNHTTIEIGKDLNYLKDGNGTTSGI..GS
hNav1.2  1034  KALDEIKPLEDLN.NKKDSCISNHTTIEIGKDLNYLKDGNGTTSGI..GS
hNav1.1  1043  KILDEIKPLDDLN.NKKDSCMSNHT.AEIGKDLDYLKDVNGTTSGIGTGS
hNav1.3  1035  KVI.EIHE....G.NKIDSCMSNNTGIEISKELNYLRDGNGTTSGVGTGS
hNav1.6  1026  READEVKPLDELY.EKKANCIANHTGADIHRNGDFQKNGNGTTSGI..GS
hNav1.7  1008  KISREIRQAEDLN.TKKENYISNHTLAEMSKGHNFLKEKD.KISGF..GS
hNav1.4   874  APEDEKKEPPEED.LKKDNHILNHMG..............LADGP..PS
hNav1.5   990  QKPAALAAQ.....GQLPSCIATPYSPPPPETEKVPPTRKETRFEE..GE
hNav1.8   942  KAEPELVVKLPLSSSKAENHIAANT..................ARGS..SG
hNav1.9   862  NLPQQKEV........AGGCAAQSK..DIIPLVMEMKRGSETQEELGILT

                                        ABD-C
                                1103                    1129
mNav1.2  1082  SVEKYVVDESDYMSFINNPSLTVTVPIAVGESDFENLNTEEFSS.ESDM
hNav1.2  1081  SVEKYVVDESDYMSFINNPSLTVTVPIAVGESDFENLNTEEFSS.ESDM
hNav1.1  1091  SVEKYIIDESDYMSFINNPSLTVTVPIAVGESDFENLNTEDFSS.ESDL
hNav1.3  1079  SVEKYVIDENDYMSFINNPSLTVTVPIAVGESDFENLNTEEFSS.ESEL
hNav1.6  1073  SVEKYIIDE.DHMSFINNPNLTVRVPIAVGESDFENLNTEDVSS.ESDP
hNav1.7  1054  SVDKHLMEDSDGQSFIHNPSLTVTVPIAPGESDLENMNAEELSS.DSDS
hNav1.4   906  SL......ELDHLNFINNPYLTIQVPIASESDLEMPTEETDT.FSEP
hNav1.5  1033  QP....GQG.......TPGDPEPVCVPIAVAESDTDDQEEDEENSLGTEE
hNav1.8   973  GLQAPRGPRDEHSDFIANPTVWVSVPIAEGESDLDDLEDDGGEDAQSFQ
hNav1.9   902  SVPKT.........LGVRHDWTWLAPLAEEEDDVEFSGEDNAQRI.TQP
                              ▲▲  ▲   ★▲▲  ▲
```

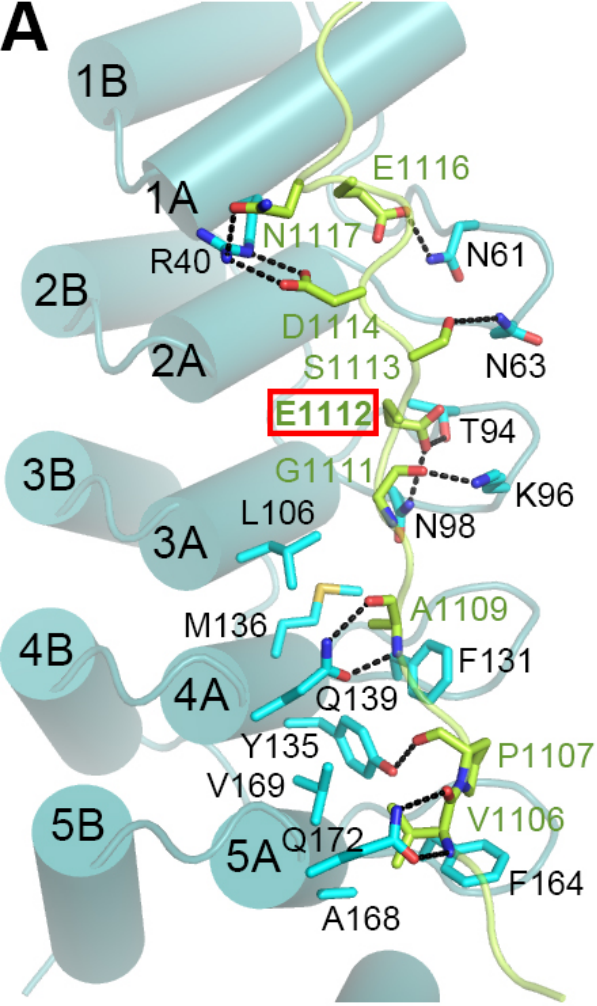

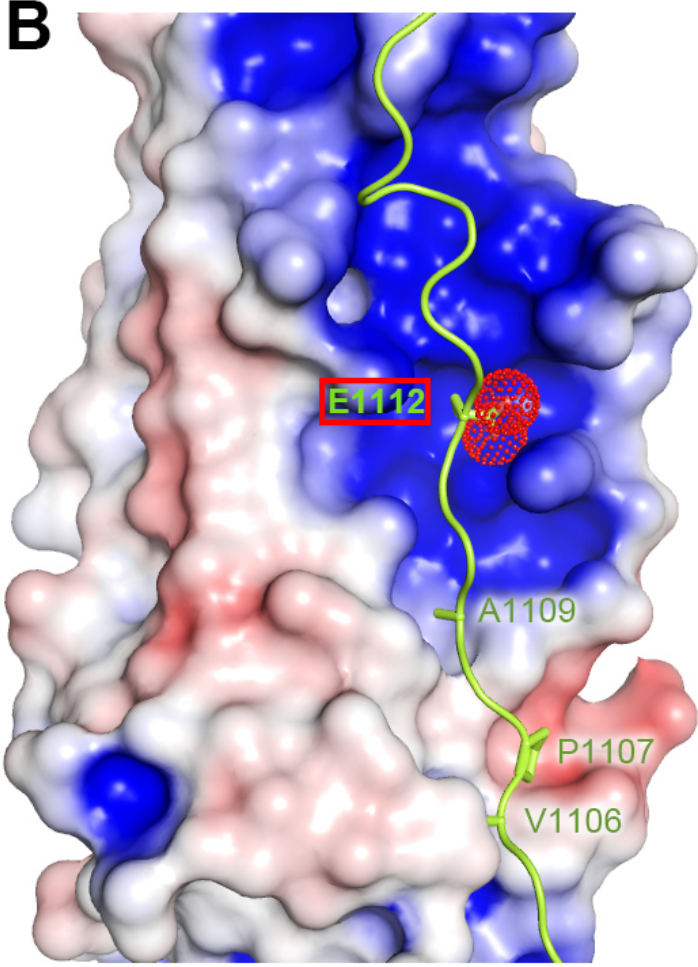

C

AnkR	1615	TPSLVTA**E**DSSLE
Nav1.2	1105	TVPIAVG**E**SDFEN
Nav1.5	1046	CVPIAVA**E**SDTDD
KCNQ2	830	RPYIAEG**E**SDTDS
KCNQ3	831	KRYLAEG**E**TDTDT
betaDG	796	VPIIFAD**E**LDDSK

D

ANK repeats	Nav1.2_ABD	K_d (μM)
WT	E1112K	>50
WT	E1112A	4.3 ±0.4
WT	E1112Q	4.6 ±0.2
T94A, N98E	WT	2.6 ±0.2

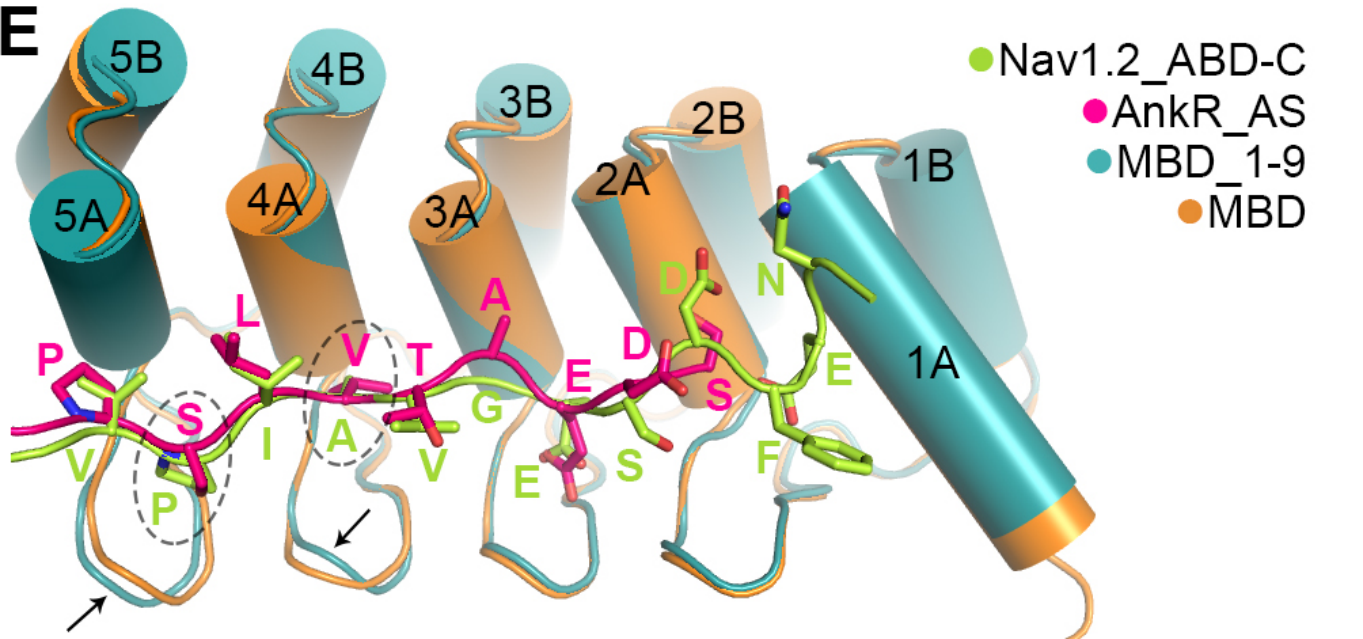

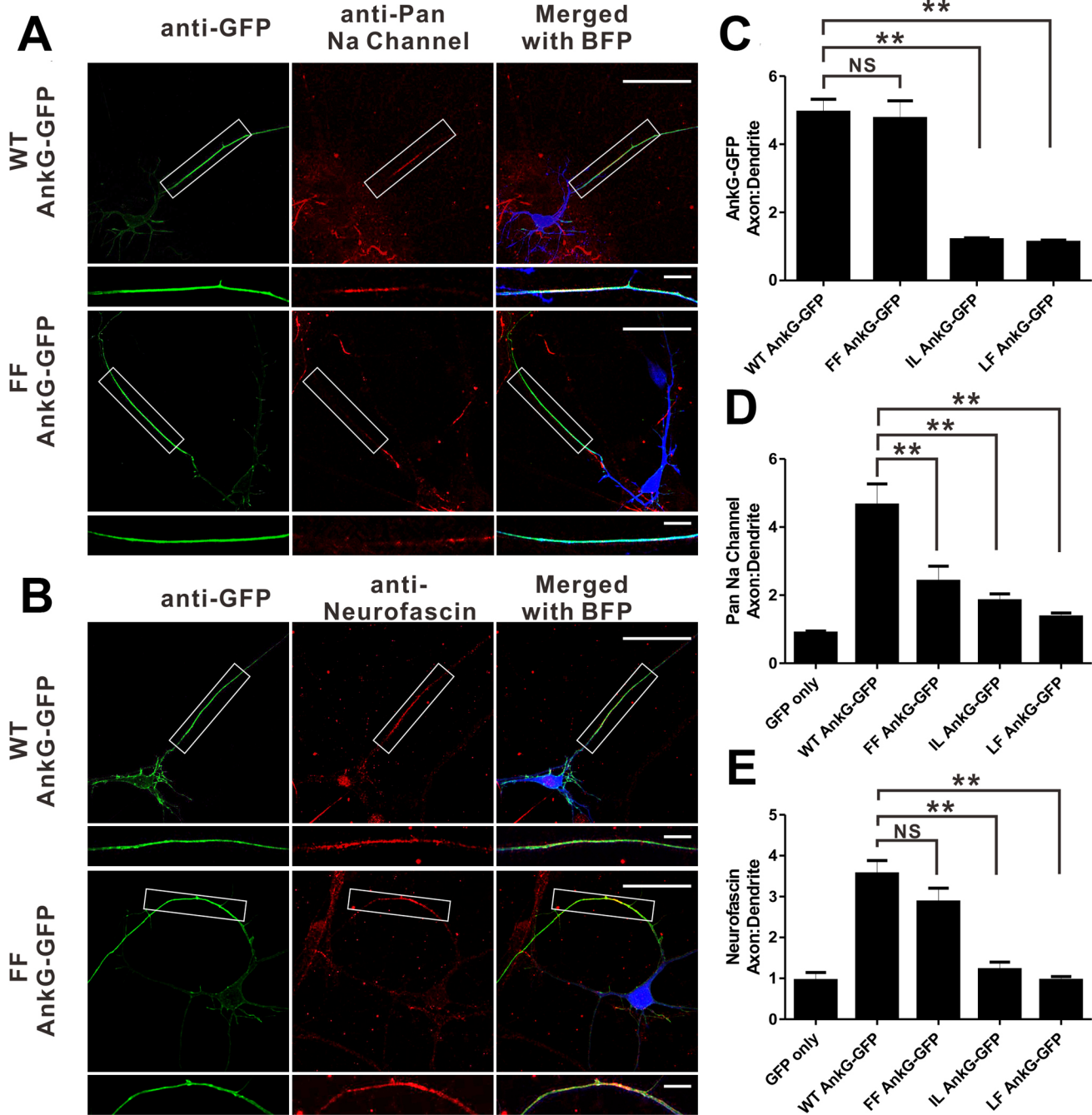
A
anti-GFP
anti-Pan Na Channel
Merged with BFP
WT AnkG-GFP
FF AnkG-GFP
B
anti-GFP
anti-Neurofascin
Merged with BFP
WT AnkG-GFP
FF AnkG-GFP
C
AnkG-GFP Axon:Dendrite
**
**
NS
0
2
4
6
WT AnkG-GFP
FF AnkG-GFP
IL AnkG-GFP
LF AnkG-GFP
D
Pan Na Channel Axon:Dendrite
**
**
**
0
2
4
6
GFP only
WT AnkG-GFP
FF AnkG-GFP
IL AnkG-GFP
LF AnkG-GFP
E
Neurofascin Axon:Dendrite
**
**
NS
0
1
2
3
4
5
GFP only
WT AnkG-GFP
FF AnkG-GFP
IL AnkG-GFP
LF AnkG-GFP